

Intraseasonal isotopic variation associated with the Madden-Julian Oscillation

Naoyuki Kurita,¹ David Noone,² Camille Risi,² Gavin A. Schmidt,³ Hiroyuki Yamada,¹ and Kunio Yoneyama¹

Received 18 October 2010; revised 19 October 2011; accepted 19 October 2011; published 17 December 2011.

[1] The Madden-Julian Oscillation (MJO) is the dominant mode of intraseasonal variability in the tropical atmosphere. This study examines the evolution of the hydrologic regime from before the onset of the MJO (pre-onset period) to the MJO onset period, using deuterated water vapor (HDO) measurements from the Tropospheric Emission Spectrometer (TES) and from ground-based stations. Ground-based observations reveal a clear transition between high HDO/H₂O isotope ratios during the pre-onset period to a period of repeated abrupt decreases in the HDO/H₂O isotope ratio associated with intense convection. Each observed minimum in the HDO/H₂O ratio corresponded to a maximum in stratiform rainfall fraction, which was derived independently from radar precipitation coverage area. The ground-based observations are consistent with the satellite observations of the HDO/H₂O ratio. In order to attribute the mechanisms that bring about the isotopic changes within the MJO convection, an isotope-enabled general circulation model (GCM) constrained by observed meteorological fields was used to simulate this MJO period. The GCM reproduced many of the observed isotopic features that accompanied the onset of an MJO. After the development of deep convection, large-scale stratiform cloud cover appears, and isotope ratios respond, as a consequence of diffusive exchange between stratiform raindrops and the surrounding vapor. In this diffusive exchange process, heavy isotopes tend to become enriched in precipitation and depleted in the surrounding vapor, and thus successive stratiform rainfall results in decreasing isotope values in the middle and lower troposphere. On the basis of these characteristics, isotope tracers can be used to partition stratiform and convective rainfall from observed isotope data and to validate the simulated proportions of convective/stratiform rainfall.

Citation: Kurita, N., D. Noone, C. Risi, G. A. Schmidt, H. Yamada, and K. Yoneyama (2011), Intraseasonal isotopic variation associated with the Madden-Julian Oscillation, *J. Geophys. Res.*, 116, D24101, doi:10.1029/2010JD015209.

1. Introduction

[2] The Madden-Julian Oscillation (MJO) is the most prominent mode of intraseasonal variability in the tropics. It is characterized by a large-scale convective envelope propagating eastward at an average speed of 5 m s⁻¹ across the equatorial Indian Ocean and reaching the western and central Pacific. The MJO also has a far-reaching influence via its interactions with other weather phenomena (e.g., the monsoon, El Niño–Southern Oscillation, and tropical cyclone genesis). Since the discovery of the MJO by *Madden and Julian* [1971], numerous studies have explored its fundamental structure and

physical mechanisms and the nature of its interactions with other aspects of the climate system, using both observation and modeling approaches (see *Lau and Waliser* [2005] and *Zhang* [2005] for a detailed review). Despite intensive research, developing a comprehensive theory that explains the characteristics of the MJO and produces reliable simulations in climate models remains a significant challenge [e.g., *Slingo et al.*, 1996; *Waliser et al.*, 2003; *Lin et al.*, 2006; *Zhang et al.*, 2006]. This difficulty stems from deficiencies in our knowledge about the MJO and requires a new framework with which to identify the mechanisms of MJO formation. In the present study, we examine the MJO from a new hydrological perspective.

[3] Recent observational analyses have explored the vertical moist thermodynamic structure of the MJO [*Kiladis et al.*, 2005; *Tian et al.*, 2006; *Benedict and Randall*, 2007; *Jiang et al.*, 2009]. These studies indicate that the space-time evolution of the MJO is linked to the hydrological cycle. In particular, *Benedict and Randall* [2007] describe the life cycle of the MJO as follows: (Stage I) Before the onset of MJO convection, enhanced solar radiation leads to low-level

¹Japan Agency for Marine–Earth Science and Technology (JAMSTEC), Yokosuka, Japan.

²Department of Atmospheric and Oceanic Science and Cooperative Institute for Research in Environmental Sciences, University of Colorado at Boulder, Boulder, Colorado, USA.

³NASA Goddard Institute for Space Studies, New York, New York, USA.

warming and moistening through surface fluxes, which promotes shallow cumuli and cumulus congestus. These lead to heat and moisture transport to the middle troposphere. This period continues for ~10–15 days, followed by a rapid transition (Stage II) to deep convection (onset period). After passage of the heaviest rainfall, stratiform precipitation appears and prolongs the MJO onset period by several days due to the stratiform instability process [Mapes, 2000]. Thus, this transition from convective to stratiform precipitation allows the MJO onset period to be sustained for ~10 days. Subsequently (Stage III), suppressed convection associated with tropospheric drying continues for approximately 10–15 days marking the end of the onset period. This observed sequence is consistent with the discharge/recharge theory, which was developed through diagnoses of the mechanisms that bring about intraseasonal oscillations in a minimal dynamical model [Blade and Hartmann, 1994; Hu and Randall, 1994; Raymond, 2001; Kemball-Cook and Weare, 2001]. However, unresolved features of the MJO remain, such as its multiscale structure and the wave triggering mechanism.

[4] To further understanding the MJO, diagnostic studies using numerical simulation are necessary. However, current global climate models still poorly represent the MJO [e.g., Slingo *et al.*, 1996; Waliser *et al.*, 2003; Lin *et al.*, 2006; Zhang *et al.*, 2006]. Limitations in model simulations of the MJO have long been considered a product of deficiencies in the treatment of cumulus convection. Thayer-Calder and Randall [2009] suggested the failure of models to produce MJO-like features results from poor representation of a realistic recharge and discharge cycle of the MJO. They argued that because modeled cumulus convection is usually triggered by the convective available potential energy (CAPE), convection is not sufficiently sensitive to the humidity in the atmospheric column. The result of this is that there is too much convection during the dry period, and the moist layer is unable to grow deeper through the entire column (moisture recharge). This explanation is consistent with a former study in which an MJO was successfully simulated by imposing moisture triggers to the deep convection schemes [Tokioka *et al.*, 1988]. In their model, Tokioka *et al.* [1988] used a minimum cumulus entrainment rate for deep convection that was expressed as a function of mixed layer depth, which ensured deep convection was suppressed until the mixed layer became sufficiently thick. To overcome the disconnection between moisture and convection in many existing convective schemes, a new cumulus parameterization was recently proposed by Chikira and Sugiyama [2010] which is characterized by a lateral entrainment rate that varies depending on the surrounding environment. Because an increase in lower tropospheric moisture by cumulus congestus can be successfully simulated by this parameterization [Chikira, 2010], its implementation is expected to improve the representation of the recharge/discharge cycle of the MJO. Additionally, improved MJO simulations have also been reported using newly available high-resolution or cloud-resolving models that do not rely on cumulus parameterization [Miura *et al.*, 2007; Khairoutdinov *et al.*, 2008; Benedict and Randall, 2009].

[5] While these new-generation models can simulate many aspects of the MJO, questions remain as to whether they can satisfactorily explain all aspects, including the longevity. A

robust diagnosis proposed by Waliser *et al.* [2009] is helpful for evaluating model performance. However, other diagnostic tools are needed to assess the movement of water associated with the recharge/discharge cycle of the MJO. Recharge involves the gradual injection of moisture into the middle and upper troposphere by convective activity while discharge is the period of intensive precipitation from stratiform cloud. Lin *et al.* [2004] showed the stratiform precipitation is particularly important to the MJO moisture and energy budgets because it contributes significantly to total intraseasonal precipitation variations. To clarify and confirm these features, it is desirable to analyze the vertical structure of hydrological variations associated with the MJO in order to distinguish the roles of convective and stratiform cloud processes. Because stable water isotope ratios in water vapor and precipitation trace differences in air mass history and condensation processes, they are used here to guide analysis of the observed and modeled hydrological cycle of the MJO.

[6] Stable isotopologues of water vapor such as HDO and H₂¹⁸O are useful tools for studying convective humidification. Their relative concentration profiles in the troposphere are sensitive to vertical water transport, condensation, and reevaporation of rainfall. Given the known constraints on isotopic exchanges associated with the processes active in the region of the MJO, the anticipated isotopic evolution associated with the recharge/discharge cycle of the MJO is illustrated in Figure 1. Because lighter isotopologues evaporate preferentially, the isotope ratio of atmospheric water vapor is lower than the ocean (i.e., the near-surface water vapor is depleted in heavier isotopes relative to the ocean liquid). During the pre-onset stage (Stage I), the moisture of oceanic origin is lifted by convection to the free troposphere and moisture is detrained from the cloud top (as the sum of clouds condensate and vapor). When the water condenses into convective clouds and precipitates, heavier isotopes preferentially condense into the cloud water/ice and the water vapor remaining in the cloud becomes more isotopically depleted. The isotopic content of water vapor thus gradually decreases with altitude, and the depleted air is detrained with the mixing of updrafts into the environment. If all the condensate is removed immediately as precipitation, the isotopic profile follows along a Rayleigh distillation curve [Dansgaard, 1964].

[7] However, isotope profiles observed in the tropics via satellite [Kuang *et al.*, 2003], balloon flight [Johnson *et al.*, 2001] and aircraft [Webster and Heymsfield, 2003] show less depletion in the middle and upper troposphere than would be predicted by a pure Rayleigh distillation process. Notably, using atmospheric trace molecular spectroscopy (ATMOS) data, Kuang *et al.* [2003] found a nearly constant isotopic profile in the upper troposphere that departed significantly from that expected from a Rayleigh distillation process. The isotopic values thus depend on how much condensed water is removed as precipitation from the rising parcel (i.e., “precipitation efficiency”). If precipitation efficiency in the convective cloud is low (condensate remains in the convecting updraft), the isotope ratio of water detrained from convective updraft is higher than would be predicted by the Rayleigh distillation process. Recent model studies confirm this explanation of the non-Rayleigh isotopic profiles [e.g., Smith *et al.*, 2006; Blossey *et al.*, 2010; Bony *et al.*, 2008] (hereafter referred to as BRV08). Thus, intense

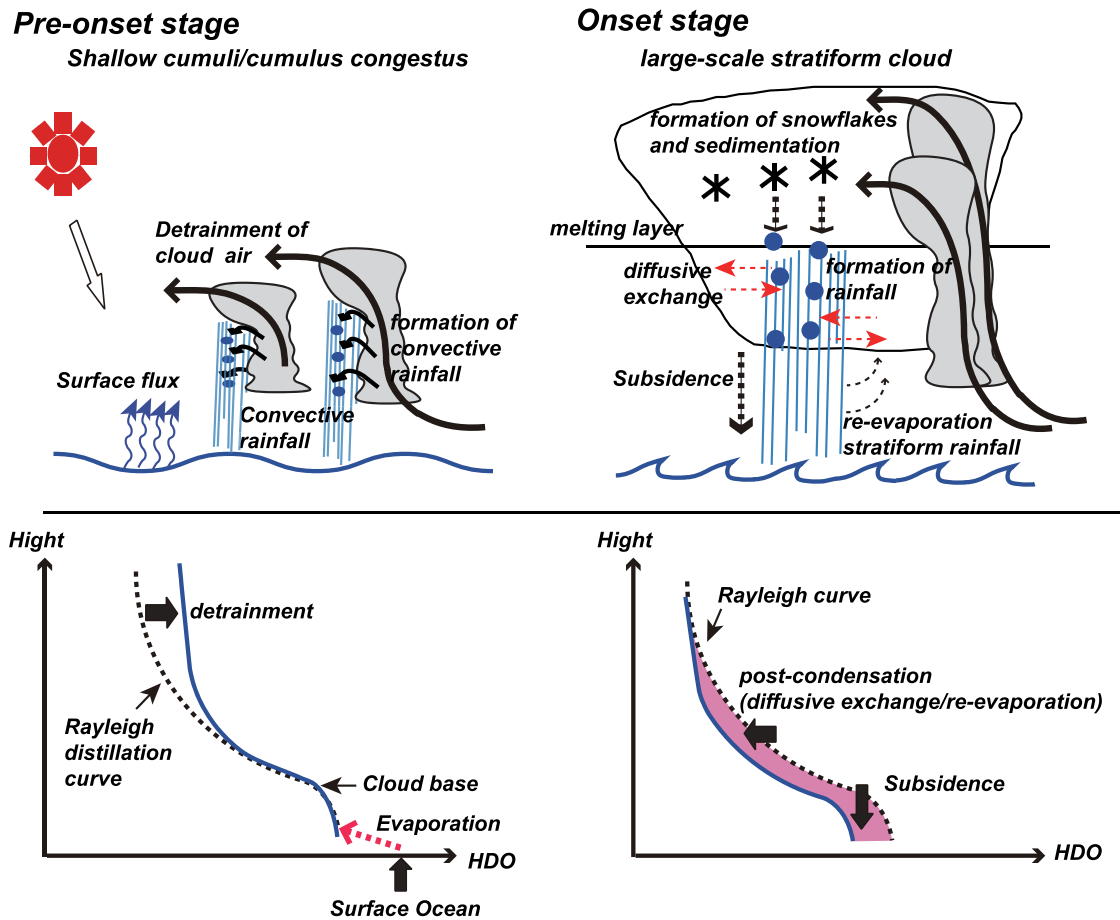


Figure 1. Schematic of vertical water transportation during the Madden-Julian Oscillation (MJO) pre-onset and onset stages. Diagrams at bottom illustrate deuterated water vapor (HDO) profile tendencies (broken lines show isotope profiles of Rayleigh distillation).

convective moistening results in a weaker vertical gradient in the isotope ratios in the troposphere. Note however, that any amount of lateral or vertical mixing of air parcels will produce departures from the Rayleigh curve [Schmidt *et al.*, 2005].

[8] During the MJO onset stage (Stage II), deep convection is accompanied by the development of large-scale stratiform cloud cover. In contrast to the influence of convective detrainment, continual stratiform precipitation acts to further decrease the isotope ratios of tropospheric moisture by the rain-out effect. In the stratiform rainfall region, post-condensation processes result in lowering the isotopic ratio of water in the atmosphere beyond that predicted exclusively from rain-out. When raindrops fall through the atmosphere, there is a diffusive exchange between the surrounding vapor and raindrops as well as evaporation of the raindrops (if the environment is unsaturated). Generally, the post-condensational exchange processes tend to result in heavy isotope enrichment in precipitation and depletion in the surrounding vapor [Lawrence and Gedzelman, 1996; Field *et al.*, 2010]. The isotopic change associated with post-condensational exchange is closely related to the intensity of falling stratiform rainfall because the degree of isotopic exchange is higher in small raindrops than in large raindrops and the mean drop size is linked to precipitation intensity. Isotopic effects in the stratiform region are also predicted to

arise as a consequence of particularly strong and widespread subsidence [e.g., Houze, 2004], which results in large-scale transport of isotopically depleted air from the upper and mid troposphere to lower altitudes. Recent satellite measurements showed more depleted HDO concentrations in the lower atmosphere than those estimated by the Rayleigh curve [Worden *et al.*, 2007]. We expect that the post-condensation effects of stratiform rainfall must contribute substantially to these depleted values, although Worden *et al.* [2007] highlighted only the influence of re-evaporation from rainfall. As shown here, the isotopic response to convective and stratiform processes differs largely and thus the isotopic content of tropospheric moisture must exhibit a distinct evolution related to the recharge/discharge process of the MJO as the dominant precipitation type changes between convective to stratiform.

[9] We use newly available satellite and ground-based observation data from the central Indian Ocean to show the isotopic variations associated with the MJO. We explore the water cycle dynamics of MJO convection with the aid of a GCM simulation that has isotopic tracers and reproduce the MJO event through a nudging technique where large-scale atmospheric information was assimilated and SSTs were prescribed. The vertical sensitivity of the TES retrieval is greatest in the middle to lower troposphere, and thus our

analysis focuses on isotopic variations below the middle troposphere. The simulated isotope field was carefully evaluated against observed data, and then the key process controlling isotopic variation during the active phase of the MJO was examined. Isotope concentrations are expressed by delta δ notation:

$$\delta = \left(\frac{R_{\text{sample}}}{R_{\text{V-SMOW}}} - 1 \right) \times 1000,$$

where R is the isotopic ratio ($\text{HDO}/\text{H}_2\text{O}$ and $\text{H}_2^{18}\text{O}/\text{H}_2^{16}\text{O}$), and V-SMOW is Vienna Standard Mean Ocean Water.

[10] The observational data are presented in section 2. In section 3, the model and experimental design is described. In section 4, the observed isotopic variation associated with MJO convection is identified. In section 5, we discuss the key process controlling the observed isotopic response to MJO convection using the nudged simulation. We also discuss how isotope tracers are particularly useful in improving the GCM representation of tropical convection when combined with the appropriate observational constraints.

2. Observational Data

2.1. Ground-Based Station

[11] The Mirai Indian Ocean Cruise for the Study of the MJO-Convection Onset (MISMO) field campaign was carried out from October to December 2006 in the equatorial Indian Ocean. In the MISMO campaign, an observation network was constructed using the R/V *Mirai* and a land-based site in the Maldives. Various meteorological and oceanographic data were obtained throughout the campaign. The MISMO sounding array data were also collected from the R/V *Mirai* (anchored at 0° , 80.5°E), Gan Island (0.7°S , 73.2°E), and Hullhule Island (4.2°S , 73.5°E) from 1 to 25 November 2006. After this period, the *Mirai* moved across the equatorial Indian Ocean and arrived at point 5.0°S , 95.0°E on 7 December 2006. Details of this campaign have been provided by *Yoneyama et al.* [2008]. In this study, we used shipboard X-band Doppler radar data to partition convective and stratiform precipitation and radiosonde sounding array data to describe background meteorological conditions.

[12] As part of the MISMO campaign, water sampling for stable isotope analysis was performed on the R/V *Mirai* and at the Gan Island station (0.7°S , 73.2°E). On the R/V *Mirai*, atmospheric moisture sampling was conducted using a conventional cold-trap method every 6 h at two heights above the sea surface, specifically at the foremast (15 m) and mainmast (36 m). The trapping employed a glass trap in an ethanol bath, which was thermoelectrically cooled to -100 degrees C. Precipitation was also collected every 6 h at deck height. At the Gan Island station, precipitation samples were collected every 3 h after routine precipitation measurements. Isotope analysis was performed using isotope ratio mass spectrometers: a MAT-252 isotope ratio mass spectrometer with a water equilibrium device for $\delta^{18}\text{O}$ measurements and a Delta-XP using the continuous-flow chromium-reduction method for δD measurement [*Kurita et al.*, 2009].

2.2. Troposphere Emission Spectrometer

[13] The Troposphere Emission Spectrometer (TES) is a high-resolution infrared spectrometer on NASA's AURA

spacecraft and is capable of measuring the $\text{HDO}/\text{H}_2\text{O}$ ratio in the lower troposphere [*Worden et al.*, 2006, 2007]. The horizontal footprint of the observations is about 5×8 km in the nadir viewing mode, with one measurement approximately every 250 km along each orbit track and 16 Sun-synchronous orbits per day. In the nadir view, TES estimates of the $\text{HDO}/\text{H}_2\text{O}$ ratio are most sensitive between 600 and 700 hPa with decreasing sensitivity to the ratio with altitude. For this study, we used TES Version 4 nadir-view global survey observations from September 2006 through February 2007 between 5°N and 5°S . Because the sensitivity to the $\text{HDO}/\text{H}_2\text{O}$ ratio depends on temperature, water content, and cloud conditions, poorer quality data are typically found when the mean temperature or water concentration is very low, thick clouds are present, or strong near-surface temperature inversions occur over land [*Worden et al.*, 2006; *Lee et al.*, 2011]. To ensure only high-quality data was used, we followed the quality control protocol used in previous studies [*Worden et al.*, 2006, 2007] and excluded data if the degree of freedom for the signal in the joint retrieval of HDO and H_2O from the TES infrared spectral measurements was less than 0.5. This criterion tended to remove measurements under high cloud optical depth, and thus TES estimates of the $\text{HDO}/\text{H}_2\text{O}$ ratio are weighted toward retrievals from clear sky conditions. The error in individual HDO measurements is around 1% in the tropics. Additionally, *Worden et al.* [2006] suggested that there is a bias in TES δD due to the uncertainty of HDO spectroscopic line strengths. In the present study, we corrected a bias in the TES $\text{HDO}/\text{H}_2\text{O}$ ratio of approximately 4–5% following *Worden et al.* [2011]. The $\text{HDO}/\text{H}_2\text{O}$ ratio is expressed in δ notation relative to V-SMOW. To construct maps, daily averaged data were binned on a $5^\circ \times 5^\circ$ longitude/latitude grid, which is approximately consistent with the longitudinal separation of the orbit track data. The comparison between modeled and TES-observed data are done following *Worden et al.* [2011] (see Appendix A). We applied the TES-averaging kernels together with an a priori profile to our model output, producing modeled δD values that are directly comparable to those measured by TES.

3. Model and Experimental Design

3.1. MIROC3.2

[14] We used the Center for Climate System Research (CCSR)/National Institute for Environmental Studies (NIES)/Frontier Research Center for Global Change (FRCGC) atmospheric general circulation model (AGCM) [*Numaguti et al.*, 1997; *Hasumi and Emori*, 2004], which is the atmospheric component of the Model for Interdisciplinary Research on Climate (MIROC) version 3.2 used in the Fourth Assessment Report of the Intergovernmental Panel on Climate Change. Cloud processes in the model are separated into cumulus convective processes and stratiform clouds. For the cumulus parameterization, the model uses the Arakawa-Schubert (AS) scheme with prognostic closure [*Arakawa and Schubert*, 1974; *Pan and Randall*, 1998]. The stratiform cloud scheme is based on that of *Le Treut and Li* [1991], in which the cloud condensate content is calculated using a total water budget equation including condensation, precipitation, ice cloud sedimentation, and evaporation of both cloud water and raindrops. The cloud condensate derived from stratiform

clouds is generally larger than that of convective clouds by an order of magnitude. Anvil clouds are treated as stratiform clouds in this model.

3.2. Implementation of Stable Water Isotopes

[15] The isotope scheme incorporated into the model is similar to that implemented in previous GCM studies [e.g., Hoffmann *et al.*, 1998; Schmidt *et al.*, 2005]. Water isotopologues (H_2O , H_2^{18}O , HDO) are transported identically in the model using dynamic processes, and isotopic ratios are conserved as long as no phase changes occur. When a phase change occurs, isotopic fractionation can take place, and isotopes are redistributed between vapor and liquid or ice crystals according to the isotopic fractionation factor. When a phase change occurs under saturated conditions, thermal equilibrium fractionation coefficients are calculated. However, non-equilibrium (kinetic) fractionation can occur under unsaturated or supersaturated conditions (see Jouzel [1986] for a detailed review).

[16] When water vapor evaporates from open water to unsaturated air, non-equilibrium fractionation is introduced and isotopic evaporation flux is computed following Merlivat and Jouzel [1979]. In cloud processes, when vapor condenses to liquid form (at temperatures higher than -5°C), equilibrium fractionation is assumed to occur between droplets and residual water vapor. Ice crystals form under supersaturated conditions when water vapor condenses to ice, introducing a kinetic fractionation following Jouzel and Merlivat [1984]. This fractionation factor is highly dependent on supersaturation conditions, which are parameterized as a function of temperature as follows: $S = 1 - \lambda * T$ (where λ is the tuning parameter, and T is air temperature ($^\circ\text{C}$)). In this model, we use the same value ($\lambda = 0.003$) utilized in other models [e.g., Hoffmann *et al.*, 1998; Schmidt *et al.*, 2005].

[17] As precipitation falls below the height of the clouds, isotopic exchange takes place through re-evaporation and diffusion with falling precipitation. When precipitation falls through the cloud, diffusive exchange of water isotopes occurs between surrounding vapor and raindrops. Diffusive exchange with ice can be ignored because diffusivity in ice is very low. There is no description of a drop size spectrum for this model, so we followed the scheme proposed by Hoffmann *et al.* [1998] in which drops from stratiform clouds are assumed to be primarily small, and 95% of rainfall reaches isotopic equilibrium before arriving at the surface. In contrast, convective shower rainfall is composed of large raindrops, and only 50% of these raindrops reach equilibrium. When precipitation falls through unsaturated air, re-evaporation of raindrops occurs which imparts a kinetic fractionation. Stewart's theory [Stewart, 1975] is often used to estimate the isotopic changes of condensate and vapor associated with re-evaporation and exchange process in the unsaturated atmosphere. These processes play an important role in isotope hydrology of the dry atmosphere, however their impact may be limited in the present study because the atmosphere over the tropical ocean is fully moistened during the convectively active period. Therefore, to simplify interpretation of the model output, we assumed that re-evaporation under the cloud base did not fractionate and that the isotopic content of re-evaporation flux was the same as that of rainfall. These assumptions likely result in a bias toward systematically higher isotope ratios in the lower atmosphere.

3.3. Simulation

[18] The model resolution in this study was T106 spectral truncation ($1.1^\circ \times 1.1^\circ$ in a Gaussian grid resolution) including 40 vertical layers, with the top level reaching 0.4 hPa. The model was run using prescribed SST and sea ice distribution [Rayner *et al.*, 2003]. The SST and sea ice distribution for each time step were computed through interpolation of mean monthly data. A nudging technique was used to assimilate horizontal wind velocity (up to 100 hPa) into the MIROC 3.2 model in order to simulate realistic atmospheric circulation. The nudging method is similar to that used in earlier companion papers [Takemura *et al.*, 2002; Kurita *et al.*, 2005; Uno *et al.*, 2009]. In this study, horizontal 6 hourly wind data from the Japan Meteorological Agency (JMA) Climate Data Assimilation System (JCDAS) [Onogi *et al.*, 2007] were used to constrain the model. The simulation started in January 1979 and was run until 2008, and was analyzed for the period between September 2006 and March 2007.

4. Observed HDO Variation Associated With the MJO

4.1. Ground-Based Observation

[19] Ground-based water isotope measurements performed intensively during the MISMO field experiment captured a weak MJO event. The MISMO observation period extended from a convectively inactive phase (pre-onset stage) to an active condition (onset stage). A time series of water budget components shows that successive strong convergence and convective rainfall events were initiated on 15 November and continued during the observation period (Figure 2). As also shown by Lawrence *et al.* [2004], the observed δD values in vapor exhibited clear intraseasonal isotopic variations associated with organized deep convection. Relatively high δD values were observed during the pre-onset stage, and repeated abrupt δD decreases appeared after onset (see Figure 3b). During the pre-onset stage, convective rainfall was dominant, but during the onset stage, an increasing percentage of stratiform rainfall within the radar observation coverage area ($80,000 \text{ km}^2$) was noted, and maximum values of this field corresponded with the lowest values of δD in surface water (labeled A-D in Figure 3). Figure 4 shows a statistically robust ($p < 0.01$) gradual decrease in δD associated with increasing stratiform area.

[20] The increased stratiform area was closely related to the MJO envelope cloud structure, which was composed of several cloud clusters propagating both eastward and westward [e.g., Nakazawa, 1988; Mapes and Houze, 1993; Hendon and Liebmann, 1994]. Yamada *et al.* [2010] found eastward-moving mesoscale convective systems (MCSs) accompanied by substantial fields of trailing stratiform clouds during the MISMO period. The zonal wind component consisted of mid-level easterlies overlying surface westerlies. Thus, anvil clouds trail to the west of the eastward propagating center of deep convection and they can be seen as a westward-moving cloud system. In Figure 5, the evolution of δD values in surface water vapor and precipitation observed during the MISMO campaign are shown along with the identified eastward- and westward-propagating systems. On the basis of the findings of Yamada *et al.* [2010], we classified all precipitation events during the MISMO period into two

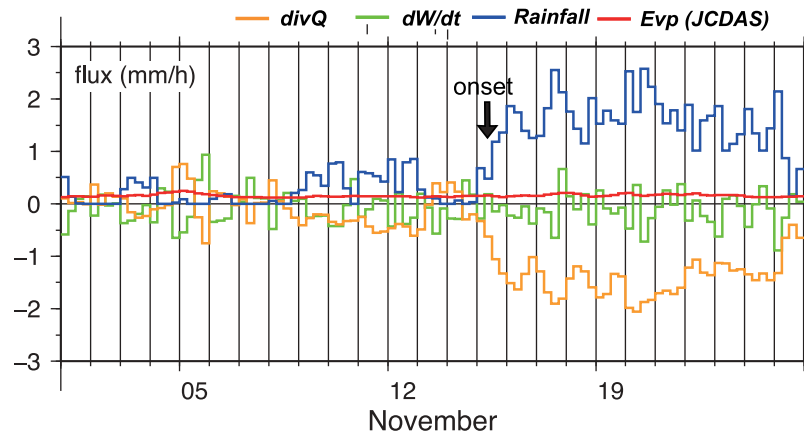


Figure 2. Time series of daily components of water fluxes calculated over the Mirai Indian Ocean Cruise for the Study of the MJO-Convection Onset (MISMO) atmospheric sounding array. The rainfall field was estimated from the water balance of the atmospheric water column above the region. The Japan Meteorological Agency (JMA) Climate Data Assimilation System (JCDAS) data set, which was obtained from the JMA at $2.5^\circ \times 2.5^\circ$ resolution, was used to calculate the precipitation field [Onogi *et al.*, 2007].

categories: rainfall associated with an eastward-propagating precipitating system (EPI) and rainfall associated with a westward-propagating cloud shield (WSI). These systems were identified through time-longitude cross-sections of surface rainfall (IR brightness temperature of the cloud top in Figure 5b) along the equator. The maximum value of rainfall (minimum cloud-top temperatures in Figure 5b) was extracted at each longitude, and a regression line was obtained using the least squares method.

[21] The maximum stratiform cloud area mentioned earlier corresponded to the merger of the two precipitation classes (EPI + WSI) (labeled A–D and Y in Figure 5b). As shown by Yamada *et al.* [2010], the WSI is characterized by moist conditions in the middle and upper troposphere, and thus the impact of convective suppression due to the entrainment of dry air is relatively weak. This situation provides favorable conditions for deep convection coupled with large-scale stratiform clouds. Additionally, lower isotope ratios in the lower troposphere were accompanied by a temperature decrease (Figure 3f). This suggests that cooled air under the stratiform cloud reached the boundary layer. As shown in Figure 5c, TES δD values in the mid troposphere (618 hPa) were much lower than those of boundary layer moisture. The increasing contribution of air subsiding from the mid troposphere explains the lower δD values in the boundary-layer. Because the lower isotope ratio signal penetrated downward from the top of the boundary layer, isotopic depletion was more prominent at higher elevations than near the surface (see $\Delta\delta D$ in Figure 3d). Thus, particularly low δD values in surface water vapor may reflect the intense subsidence associated with MCSs. Because zonal convergence was found to be dominant in the layer below 700 hPa [Yoneyama *et al.*, 2008], low-level moisture convergence would be the dominant source of the rainfall from these MCSs. Thus, the δD variations in surface vapor matched those of precipitation, and all δD minima in precipitation collected from both the R/V *Mirai* and Gan Island corresponded to intense EPI + WSI type rainfall (Figure 6).

[22] Following the passage of the MCSs, heavy rainfall ended and the observational region experienced calm con-

ditions, similar to those during the pre-onset period. Surface latent and sensible heat flux from the ocean were higher than during the convectively active period, which allowed for an increase in the near surface humidity. The maximum surface heat flux occurred just before the MCSs arrived (see Figure 3h). As shown in Figure 1, the isotope ratio of vapor derived from evaporation of the ocean is higher than that water vapor away from the surface [e.g., Craig and Gordon, 1965]. Consequently, once heavy precipitation stopped, surface isotope ratios reached values similar to the pre-onset as a consequence of surface evaporation flux. During the onset period, several MCSs passed through the observation area and, as a result, the δD values near the surface showed sawtooth-like oscillations. However, δD values of middle tropospheric moisture showed no significant isotopic enrichment during this period (see Figure 5c). This result suggests that moisture supply to the troposphere from the boundary layer is weak, although low-level moisture within the boundary layer is restored by surface evaporation.

4.2. Satellite Observations

[23] In this section, we extend the analysis to time and space using satellite retrievals of HDO (TES δD). Figure 7a illustrates the temporal evolution of mid-troposphere (618hPa) δD along the equator from the Indian Ocean to Pacific Ocean. As expected from the ground-based observations, there is a clear link between the MJO and the TES δD signal, in which the minima of δD correspond to minima in low outgoing longwave radiation (OLR) [Wheeler and Weickmann, 2001]. The lowest TES δD values trail to the west of the eastward propagating center of deep convection, which provides a reminder that the δD values reflect the integration of water mass changes that occur during convection and propagate westward following the background flow. Using a one-dimensional model of cumulus convection, BRV08 simulated clear intraseasonal δD variations in atmospheric moisture during the strong and organized super cloud clusters that occurred during the Tropical Ocean-Global Atmosphere-Coupled Ocean-Atmosphere Response (TOGA COARE)

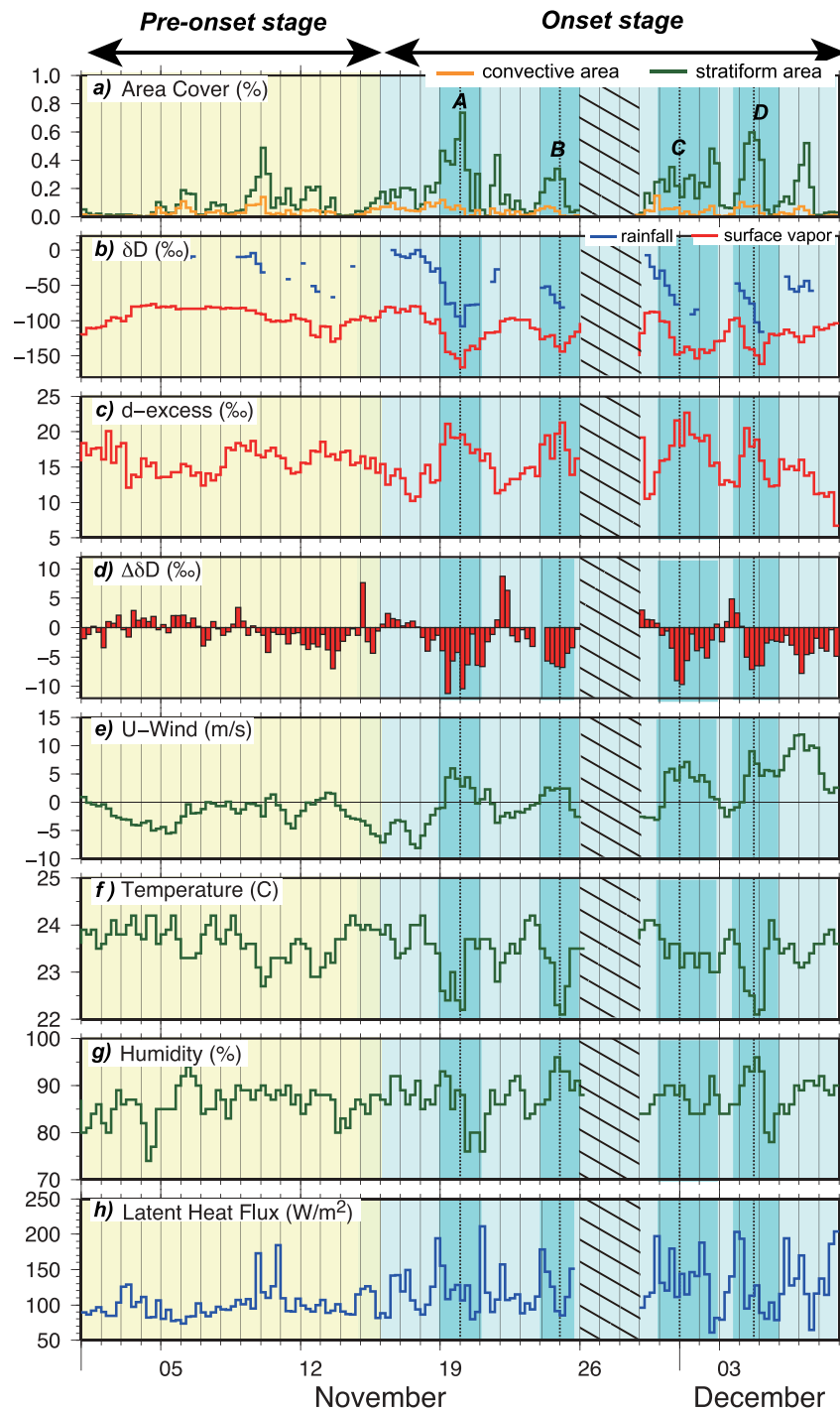


Figure 3. Time series of 6 h average isotopic values and meteorological quantities during the MISMO observation period on the R/V *Mirai*. The transition from a convectively inactive condition (shaded in yellow) to an active condition (shaded in blue) was observed around 16 December. (a) Radar echo area coverage in which reflectivity exceeds 15 dBZ for convective-type (orange) and stratiform-type (green) clouds at a height of 3 km. Total radar observation coverage was 80,000 km². (b) The δD in precipitation (blue line) and atmospheric surface water vapor at 36 m above the sea surface (mainmast height, red line). (c) The d-excess in atmospheric surface water vapor at the mainmast. (d) Isotopic difference between water vapor taken from 36 m above the sea surface (mainmast height) and 15 m above the sea surface (foremast height) (δD at 36 m $-\delta D$ at 15 m, red bar). (e) Zonal wind. (f) Air temperature. (g) Relative humidity (averaged over a 1 km height range for Figures 3e–3g; green line). (h) Estimated latent heat flux from the ocean surface. The labels A–D color-correspond to an isotopic oscillation during a convectively active period.

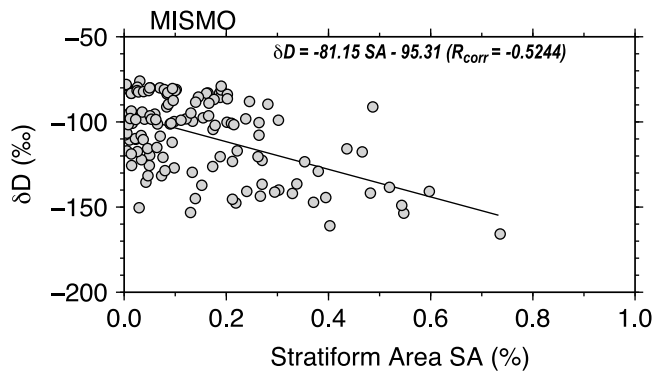


Figure 4. The relationship between 6 h average δD values of surface water and corresponding stratiform radar echo area coverage as shown in Figure 2.

experiment. Their results exhibited relatively high δD values during the period of suppressed convection; these values then decreased rapidly after the onset of convection at each level in the troposphere (see Figure 10 of BRV08). BRV08 concluded that enhanced compensating subsidence in the environment is a key process controlling these intraseasonal isotopic changes. During intense convection, upward mass fluxes at the cloud base (cloud base mass flux) increase, so the compensating downward mass flux must be accelerated in the environment. With respect to the isotope ratios, the enhanced downward mass flux transports moisture with low isotopic ratios to the lower troposphere. Downdrafts supply dry air with low δD values to the boundary layer, and results in both low boundary layer isotope ratios and a decrease in humidity during the active convection period. Their explanation is largely consistent with the observed isotopic response to the MJO convection presented here. However, MISMO data showed that the minimum isotope values lagged the maximum convection activity and corresponded to the maximum stratiform cloud region, which was not predicted by the column model of BRV08. These findings suggest that the

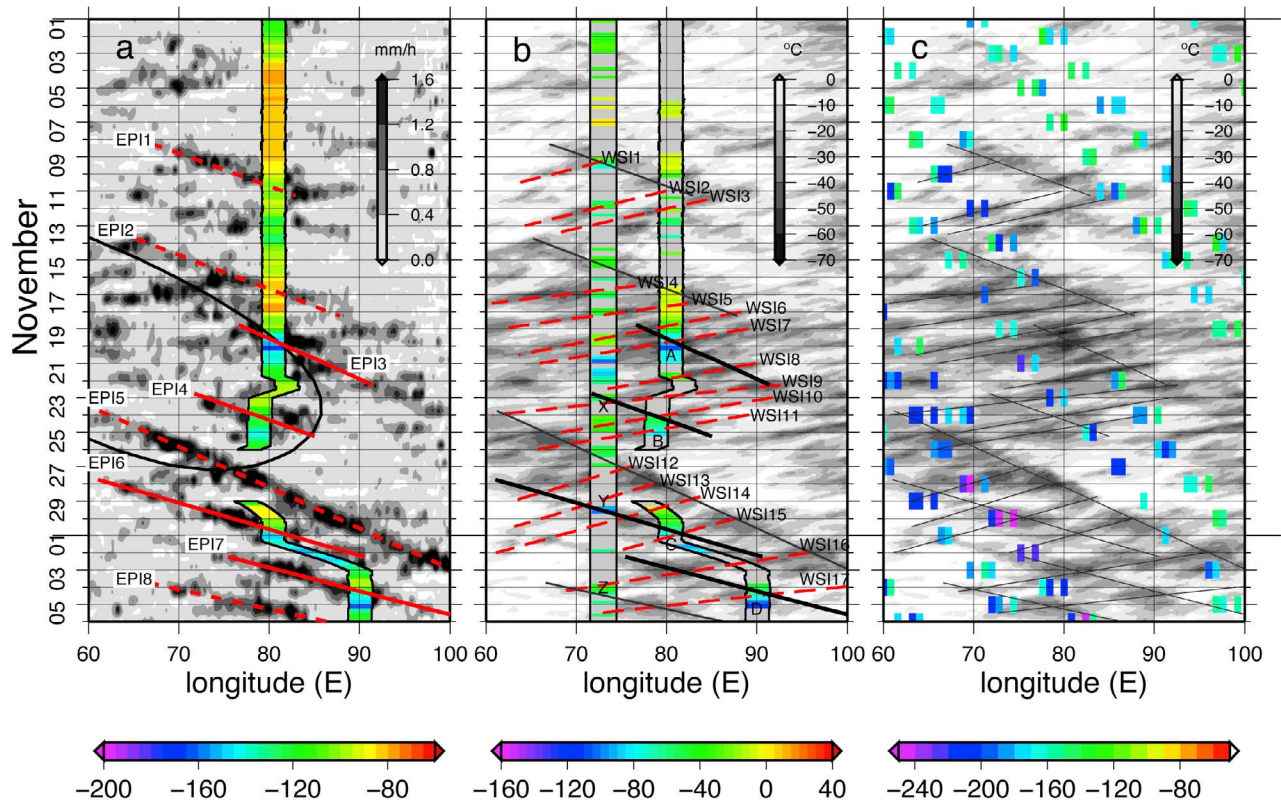


Figure 5. (a) Time-longitude section of the microwave-derived surface rainfall rate (mm/h) averaged between 5°S, 5°N, and 6 h average δD values in surface water vapor (36 m above the sea surface) at the R/V *Mirai* location. Solid and dashed lines indicate an eastward-moving precipitation system with low δD values and without these values, respectively. Black contour lines show identified MJO signals obtained from wave number–frequency filtering of OLR data [Wheeler and Weickmann, 2001]. (b) Time-longitude section of cloud-top temperature (°C) and 6 h δD values of precipitation observed at the R/V *Mirai* and Gan Island stations. Solid and dashed lines indicate identified eastward-moving precipitation systems and westward-moving cloud shields, respectively. Where the EPI and WSI with low δD values intersect are labeled A–D and X–Z. (c) TES δD values at 618 hPa (resolution: 5×8 km) are superimposed on Figure 5b.

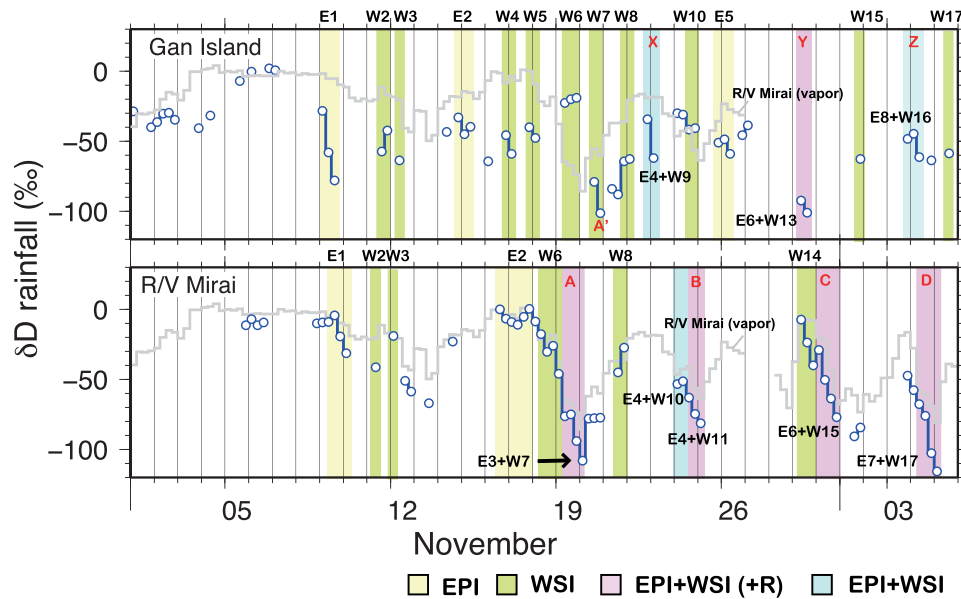


Figure 6. A time series of δD during precipitation events (blue open circles) observed at the R/V *Mirai* and Gan Island stations. Time series of δD in surface water vapor from the R/V *Mirai* (gray line) are also shown. Background color bars indicate the following classified rainfall types: eastward-propagating precipitation system (EPI, yellow), westward-propagating cloud shield system (WSI, green), EPI + WSI with intense rainfall (light purple), and EPI + WSI with no intense rainfall (light blue). The characters labeled A-D and X-Y are the same as in Figure 5b. A' corresponds to the area downstream of A along WSI7 in Figure 5b.

depleted TES δD signal during the onset of the MJO convection is associated mainly with stratiform cloud cover.

5. Model Simulation

5.1. Comparison With TES δD

[24] We use results from the nudged GCM simulation to clarify the mechanisms responsible for the isotopic depletion within and near a convective system. First, to assess the model performance, the simulated δD field was compared with TES δD values. Figure 7 illustrates simulated longitude-time diagrams of δD values of atmospheric water vapor at 618 hPa together with TES-retrieved δD values. Although a bias correction was performed, the simulated minimum and maximum in δD values show a systematic positive bias of 25‰ compared to TES δD values. This systematic offset has been reported in the comparison with another GCM (C. Risi et al., Process-evaluation of tropospheric humidity simulated by general circulation models using water vapor isotopologues: 1. Comparison between models and observations, submitted to *Journal of Geophysical Research*, 2011), and it remains unclear if this is associated with model error or the need for better accounting of the spectroscopic uncertainty in the TES data. As for intraseasonal variability, the model reproduced the low δD values during the active convection, however the prominent and sustained high δD values observed during the inactive phase were not reproduced by the model. Therefore, the transition from high δD values during the convectively inactive phase to the period of low δD values associated with active convection was smaller than that of TES (see Figure 7b).

[25] In the GCM, cumulus convection (AS scheme) is controlled by the cloud work function, which is roughly equivalent to CAPE. Convection occurs whenever positive CAPE exists. As noted earlier, this type of formulation is known to produce deep convection too frequently and consequently poorly resolves the moistening process during the pre-onset period. During the pre-onset phase, TES δD observations suggest that surface evaporation supplies vapor of relatively high δD values to the atmosphere and then this isotopically enriched air is transported to the middle troposphere by shallow convection and cumulus congestus with low precipitation efficiency. Low precipitation efficiency is identified circumstantially by considering that the high isotopic ratios occur because the isotopic depletion due to rain-out is small. However, in the GCM, convective rainfall occurs and removes heavy isotopes from the atmosphere. Thus the modeled increase in the isotope ratio of middle tropospheric moisture is too weak. Additionally, intense deep convection would cause moistening in the upper troposphere, which would provide favorable conditions for stratiform cloud formation. As mentioned in section 1, stratiform cloud processes act to decrease the δD values in the atmospheric water. Thus, the failure of the model to realistically represent the moisture recharge process results in the simulated δD values in the middle of troposphere during the convectively inactive phase that are too low. This in turn may be linked to the inability of the model to reproduce MJO events without nudging.

5.2. Vertical Isotopic Profile

[26] Figure 8 shows the vertical δD profiles in an environment in which convective or stratiform precipitation was

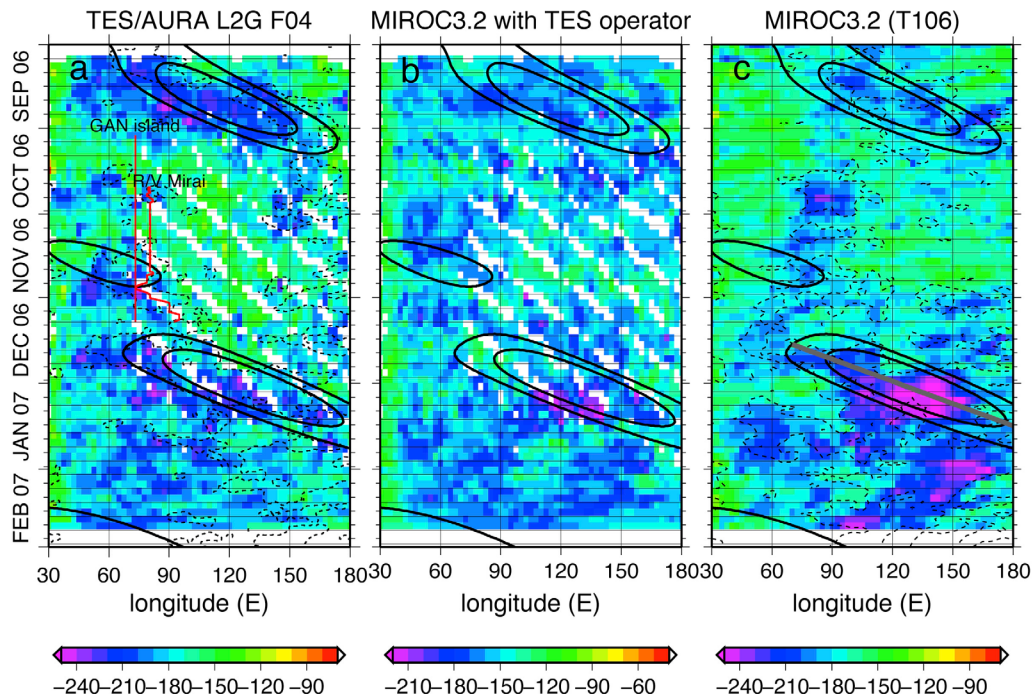


Figure 7. (a) Time-longitude cross section of the daily averaged TES δD values at 618 hPa from September 2006 to February 2007. The data are gridded for plotting using a nearest neighbor algorithm, which computes a weighted mean value within a radius of 500 km. The broken-line contours correspond to the deep convective cloud area (outgoing longwave radiation (OLR) $< 210 \text{ W/m}^2$). Solid-line contours show identified MJO signals obtained from wave number-frequency filtering of OLR data [Wheeler and Weickmann, 2001]. The positions of the R/V *Mirai* and Gan Island stations are shown, with isotope observations as red lines. (b) The same as in Figure 7a, except showing the nudged GCM simulation output. TES averaging kernels were convolved with the model output. The solid-line contour of the MJO is the same as that in Figure 7a. (c) The same as in Figure 7b, except showing the nudged GCM simulation at 627 hPa without convolution of the averaging kernel. The broken-line contours correspond to the deep convective cloud area (outgoing longwave radiation (OLR) $< 210 \text{ W/m}^2$). The solid-line contour of the MJO is same as that in Figure 7a.

dominant (the fraction of convective/stratiform precipitation exceeds 0.8). Although the humidity profile is similar between the convective and stratiform rainfall regions, the δD values of the convective rainfall region were higher through the whole troposphere. One of the robust features of the convective atmosphere is that the δD values increase with altitude at elevations higher than the 600 hPa pressure level. In the free troposphere, convective detrainment is one of the major sources of water vapor. Figure 8 shows that moisture detrained from convective updrafts is relatively enriched in heavy isotopes compared with environmental values. Below the 600 hPa level, δD values are less than those at 550 hPa because our model cannot represent cumulus congestus during the convectively inactive period. As pointed out by BRV08, strong convective updrafts transport condensed water upward before it precipitates, resulting in less depleted δD in water vapor than in an adiabatically ascending air parcel. The degree of δD depletion in the convective updraft is affected by the precipitation efficiency, which is defined as the ratio of condensate converted to precipitation compared to total condensate. As shown in Figure 8 (right), the rate of decrease in δD with altitude becomes smaller when precipitation efficiency is lower (broken gray lines).

[27] In contrast, in the stratiform rainfall region, preferential removal of heavy isotopologues due to rain-out occurs in the middle troposphere. Post-condensation processes, such as isotopic exchange with falling precipitation, also contribute to the lower isotopic values in the water vapor. Additionally, under the cloud base, diabatic cooling by evaporation from stratiform rainfall enhances subsidence and transports moisture with depleted isotopic values to the lower atmosphere. In the stratiform precipitation area, several factors can contribute to more depleted δD values than under clear sky conditions. The large isotopic difference between convective and stratiform rainfall largely relates to the simulated transition from high δD during the pre-onset period to a period of low δD associated with the MJO convection.

5.3. Simulated δD Signal Associated With the MJO Convection

[28] As shown by observed data in Figure 7a, the nudged simulation indicated a clear link between the simulated δD values and the slow eastward propagation of organized deep convection (the broken contour lines show OLR less than 210 W/m^2). The phase speed was similar to that of the MJO, although the deep convective cloud area seemed to be

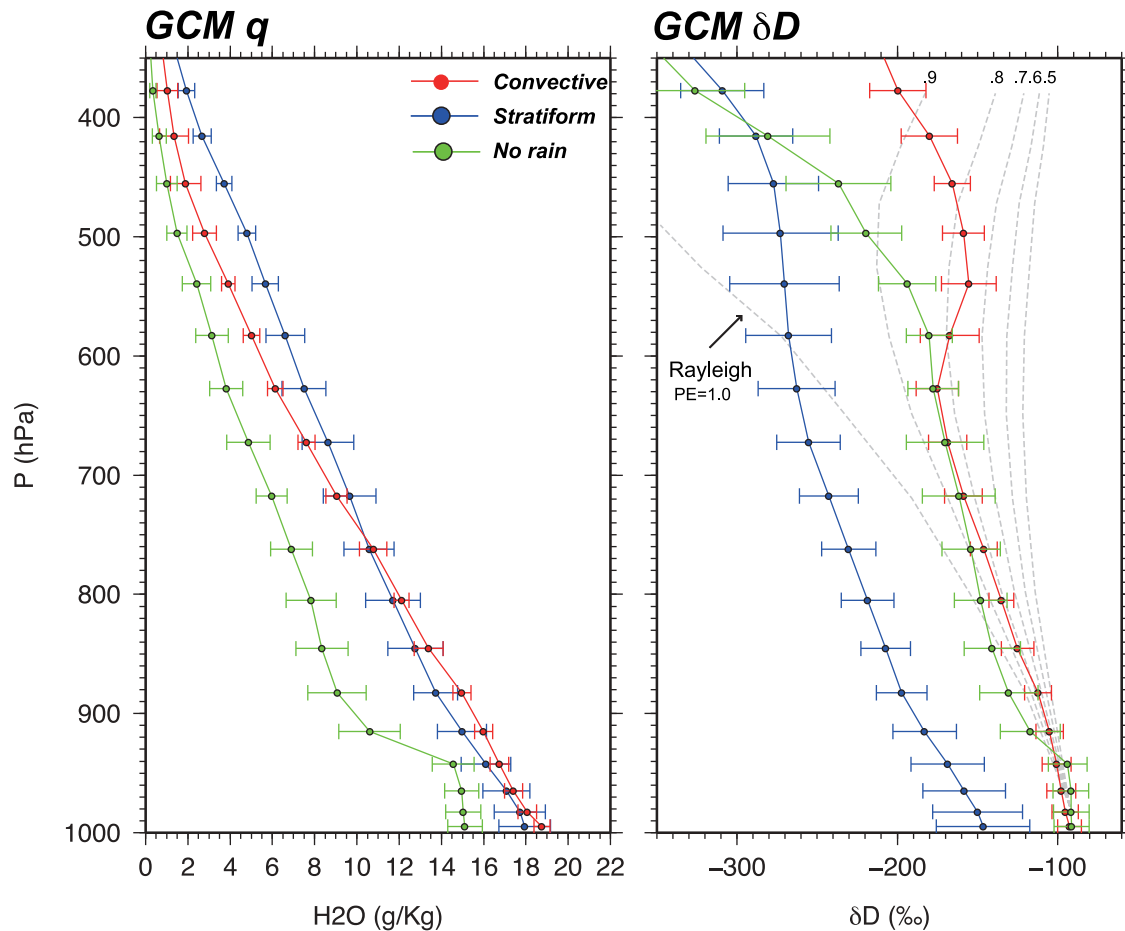


Figure 8. (left) The vertical profile of humidity (g/kg-air) in the convective rainfall region (red line), and in the stratiform rainfall region (blue line), and under clear sky (green line). The convective/stratiform rainfall region is where the proportion of convective/stratiform rainfall to total precipitation exceeds 0.8 in the area of Figure 10 from 20 December 2006 to 20 January 2007. Error bars show the standard deviation. (right) Same as Figure 8 (left) except showing δD data. The broken grey lines show total water (sum of vapor and cloud condensate), computed by assuming some of the condensate to remain as cloud, and the remainder to fall as precipitation [Jouzel, 1986]. The fraction that remains as cloud is a measure of precipitation efficiency (PE). The case where no condensation remains (PE = 1.0) corresponds to classical Rayleigh distillation.

overestimated in the simulation (see broken contour in the Figure 7c). A clear signal of the MJO initiation is shown in mid-December in Figure 7c. The MJO event started in the Indian Ocean and moved eastward over the Indian Ocean and Maritime Continental (MC) region (100°E – 150°E). The longitude-height plot of simulated δD along the gray line in Figure 7c exhibits remarkably low δD values in the middle atmosphere (around the 627 hPa) between Indonesia and New Guinea (120°E – 150°E) (Figure 9a). Furthermore, the higher d-excess values (d-value), defined by Dansgaard [1964] as $d = \delta D - 8\delta^{18}\text{O}$, of tropospheric water match the lower δD values (Figure 9b). This phenomenon will be discussed in section 5.4. In this regime, convection became weak, stratiform rainfall (large scale precipitation) became dominant (Figure 9c), and the minimum δD values of precipitation were also simulated (Figure 9d).

[29] Figure 10 shows daily δD of atmospheric moisture at 627 hPa with moisture flux (Figure 10, left) and the pre-

cipitation field (Figure 10, right) when the minimum δD values were observed in Figure 9a. When the MJO convection approached the area west of the MC (100°E), relatively low δD values were seen in the intertropical convergence zone (ITCZ), which was located between 5°N and the equator over the Western Pacific (labeled WD1, WD2 and WD3 in Figure 10). The air with lower δD values in the ITCZ propagated westward following the background flow (the mean velocity of easterly flow was 5 m s^{-1} at 627 hPa). The precipitation field showed an increasing proportion of stratiform rainfall in the ITCZ region during this period. Further decreases in δD in this westward-propagating signal corresponded to the high proportion of stratiform precipitation. At the intersection between this signal and the MJO convection, the δD value reached its minimum. After the MJO event passed over the MC, convective rainfall became dominant throughout the ITCZ area, after which the depleted δD values gradually disappeared (Figure 11).

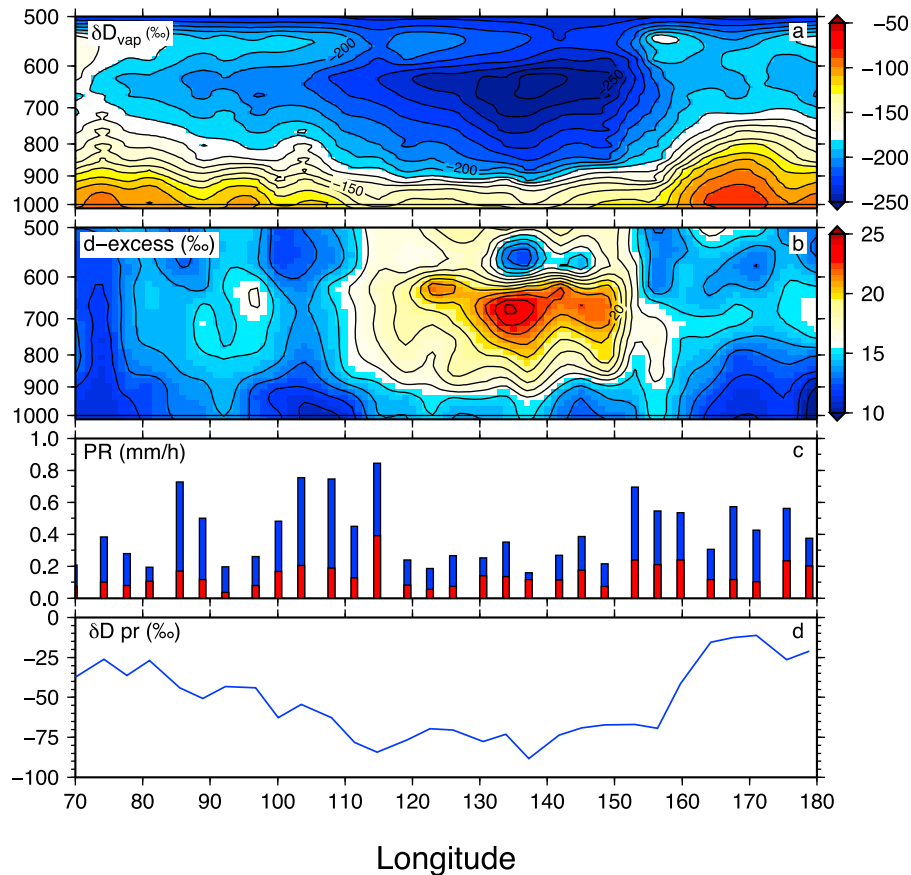


Figure 9. Simulation results along the gray line in Figure 7c. Vertical profiles of (a) δD , (b) d-excess of water vapor, (c) total amount of precipitation (blue bar) and stratiform rainfall (red bar). (d) δD of total precipitation.

[30] The relationship between the δD values of middle tropospheric moisture and stratiform precipitation amount over the MC (5°S – 5°N , 80°E – 180°E) is shown in Figure 12. In the case of a weak rainfall event ($<0.5 \text{ mm h}^{-1}$), the δD values were distributed without a clear trend in relation to precipitation amount. However, when precipitation exceeded 1.0 mm/h , the high δD values disappeared, and a clear trend between lower δD values and an increase in stratiform precipitation is evident. The decrease in isotopic ratios with increasing stratiform precipitation amount suggests that stratiform processes play an important role in the observed minima of water vapor δD . This conclusion is consistent with the result obtained from the MISO observations. Although the model could not reproduce the observed mesoscale cloud structure during the MISO period, it successfully reproduced the decrease in δD associated with the stratiform process.

5.4. Isotopic Responses to the Stratiform Precipitation Process

[31] Figure 13 presents the daily variation in the longitude-height plot of simulated δD and d-excess values (see section 5.3 for definition) of atmospheric moisture at 2.5°N (see red broken line in Figure 10 (left)) during sustained convergence associated with the MJO. Minima in the δD

values are clearly evident between 600 and 700 hPa. However, these minima do not match the maximum condensation rate. This layer corresponds to just below the melting-temperature layer, where falling snowflakes and ice crystals melt to form liquid raindrops. Below the melting layer, diffusive exchange of water isotopes takes place between surrounding vapor and raindrops. Because of the low diffusivities of ice, isotopic exchange between vapor and ice can be ignored [Jouzel and Merlivat, 1984]. In the model, this post-condensation process plays a role in producing the minimum δD values in the middle of the atmosphere.

[32] In order to reinforce the above discussion, we use the d-excess values (d-values). As shown in Figure 13, the low δD values are accompanied by the highest d-values. When the temperature is above freezing, the d-value remains relatively constant during the condensation of liquid near saturation, but the value is sensitive to the kinetic isotopic effect associated with ice condensation or when evaporation occurs at low humidity. In the GCM, the d-value in the environment generally increased with altitude, especially in the upper troposphere. The change in d-value with altitude does not result from the kinetic isotope effect during the formation of ice crystals or snow flakes under supersaturation. The rise in d-value with altitude can be seen in the model even in the absence of kinetic effects (see Figure 6 of BRV08).

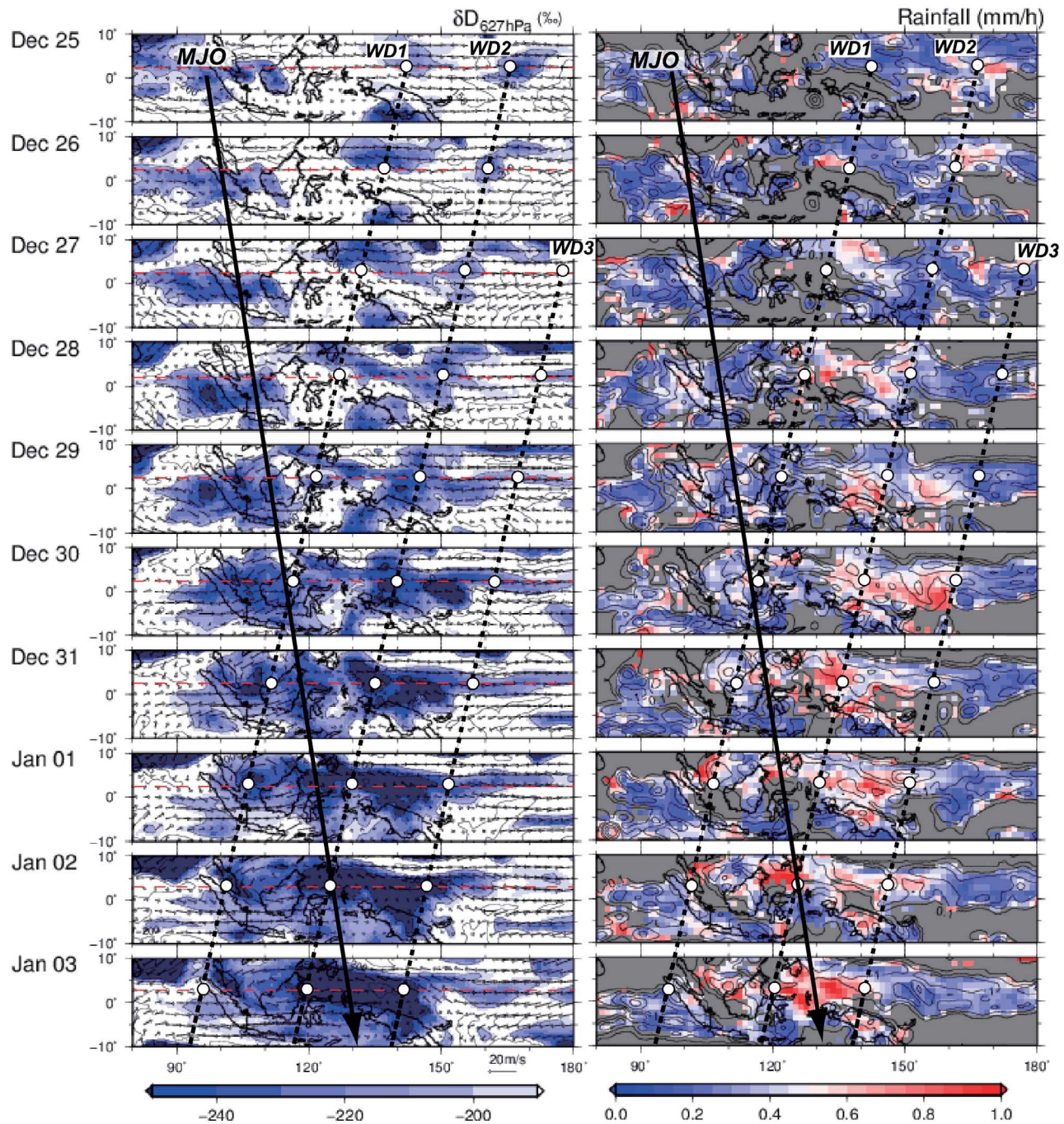


Figure 10. Daily averaged spatial distribution of (left) the simulated δD value of water vapor at 627 hPa superposed by horizontal wind and (right) total precipitation (>0.1 mm/h) from 25 December 2006 to 3 January 2007. The color of the rainfall field indicates the fraction of stratiform rainfall within total rainfall. A solid arrow indicates the movement of the MJO convection. Broken lines with white circles indicate identified westward-moving δD signals following the westerly background flow (5 m/s).

Snowflakes and ice crystals formed in the upper troposphere are labeled by high d -values, and that signature is then carried down to lower levels where the snowmelts and evaporates. Therefore, it can be used as a “tag” of subsidence.

[33] Figure 14 shows that a large amount of stratiform precipitation was formed in the upper troposphere (around 300 hPa) before the decrease in δD values in the middle

atmosphere. This process occurred in the stratiform rainfall region, and the air associated with lower δD values moved westward following the background flow. When the stratiform cloud base propagated to lower altitudes, the low δD and high d values were extended to the lower atmosphere (labeled D1–D5 in Figure 13 and Figure 14). At the intersection with the organized convection associated with the MJO propaga-

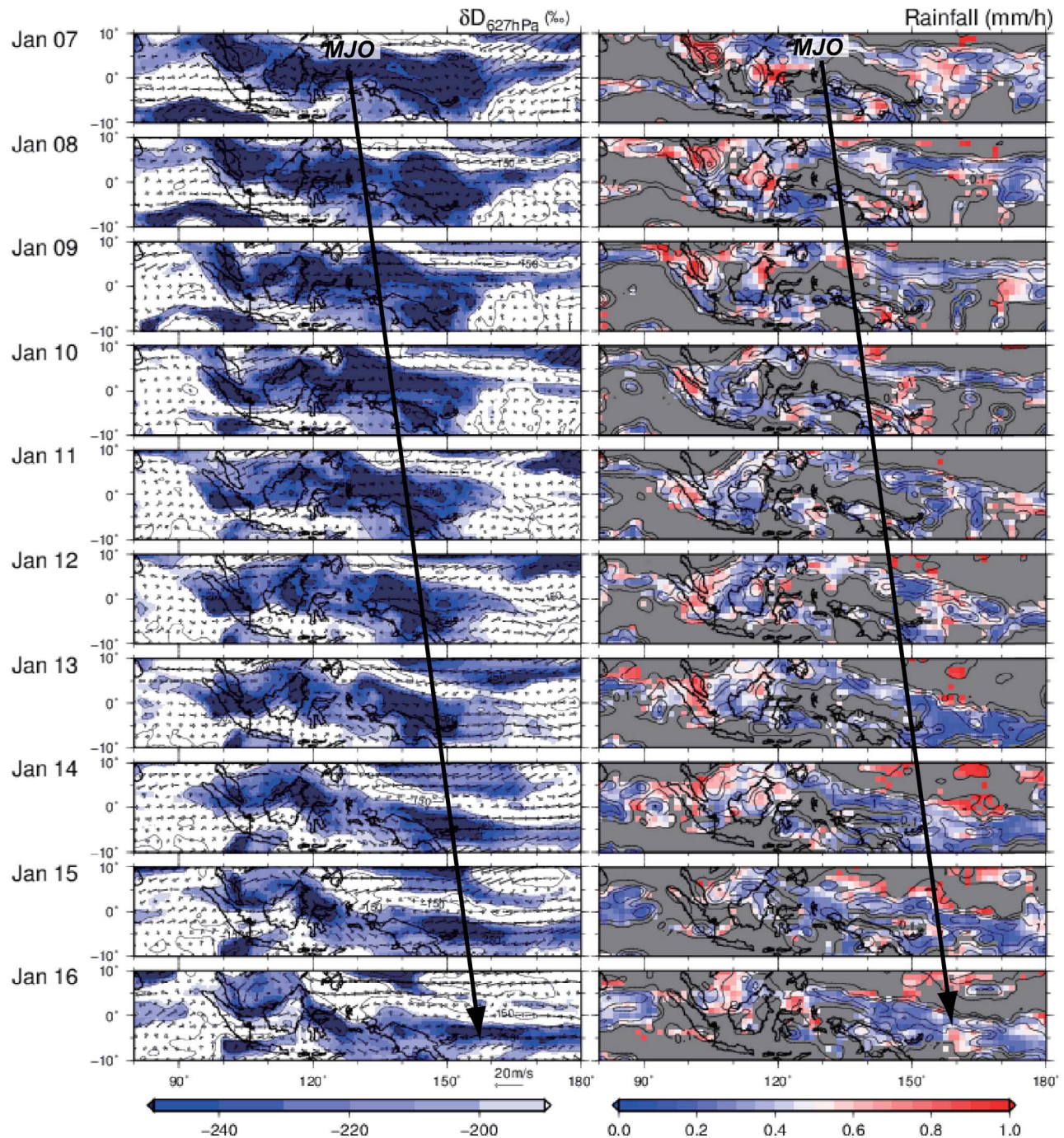


Figure 11. Same as Figure 10 but representing daily images for a subsequent time period (7 January to 16 January 2007).

tion, the influence of this downward propagation reached the surface. In the MISO observations, the lower δD values of surface moisture were also accompanied by higher d -values and exhibited a clear negative relationship ($R_{corr} = -0.57$). Under the stratiform cloud base, re-evaporation of rainfall results in higher d -values in the environmental air because of the difference in diffusivity between HDO and H₂¹⁸O [Stewart, 1975]. However, this observed δD - d -excess relationship was reasonably simulated in the model even without

the kinetic fractionation associated with re-evaporation (Figure 15).

[34] This suggests that the kinetic effects that accompany evaporation of falling rain are not the primary origin of the d -value anomaly. Instead, the d -value is acting as a tracer for condensation conditions higher in the atmospheric column. The average relative humidity under the cloud base exceeds 0.8, and the actual humidity surrounding the raindrop must be more humid due to the evaporating raindrops. Therefore,

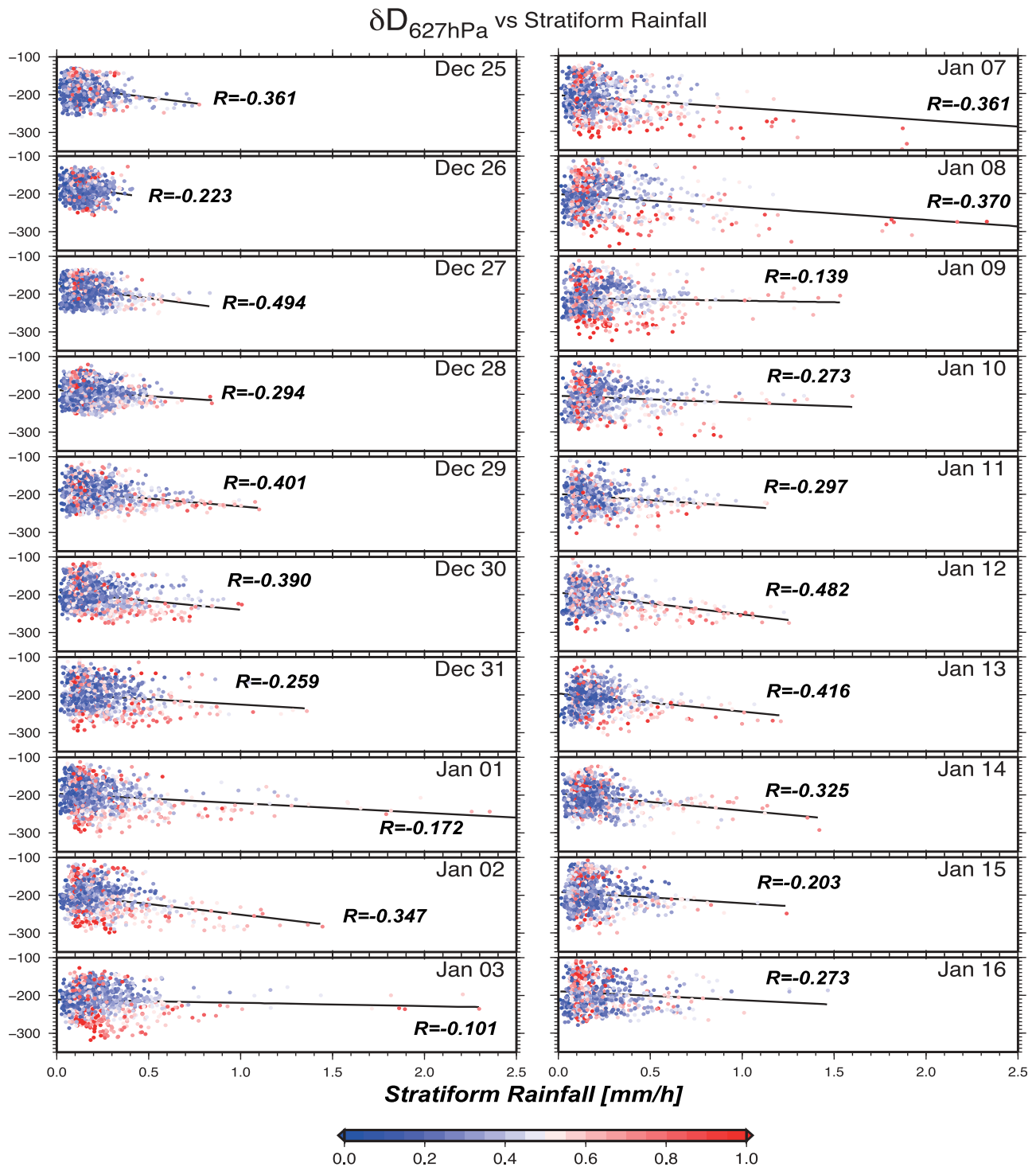


Figure 12. Relationship between the simulated daily mean δD value of tropospheric vapor at 627 hPa and stratiform precipitation amount in the area of Figure 10 from (left) 25 December 2006 to 3 January 2007 and (right) 7 January to 16 January 2007. Color indicates the fraction of stratiform rainfall to total rainfall. The regression lines were calculated only for cases in which the fraction of stratiform rainfall exceeded 0.5.

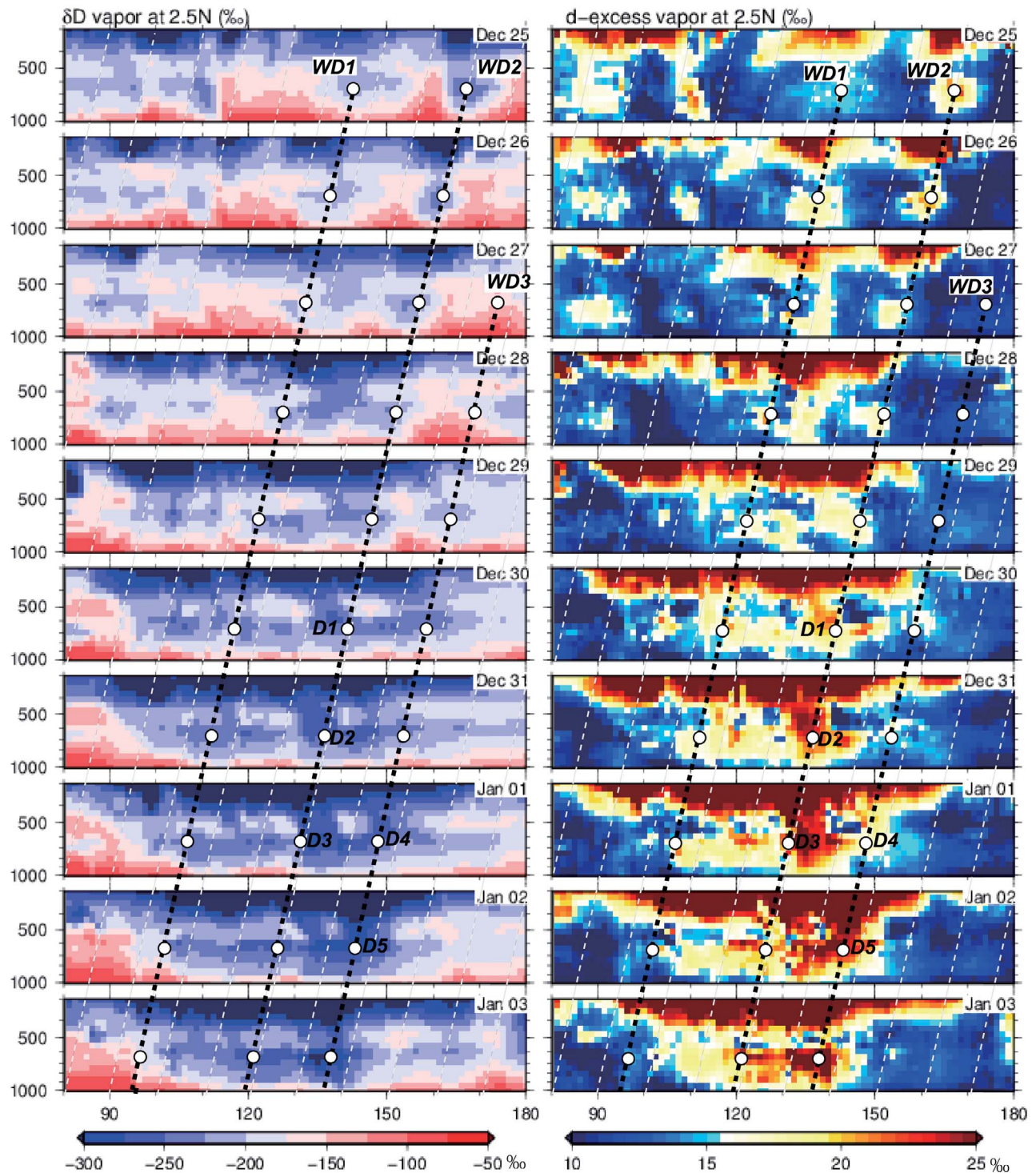


Figure 13. Vertical cross section of the GCM simulated (left) δD value and (right) d -value of water vapor sliced along the latitude 2.5°N (broken red line in Figure 10 (left)) from 25 December 2006 to 3 January 2007. Broken lines correspond to WD1–WD3 in Figure 10. White circles on the broken lines indicate at the same pressure level as in Figure 10 (627 hPa). Locations where significant decreases in the δD value and increase in the d -value at 627 hPa occurred are labeled D1–D5.

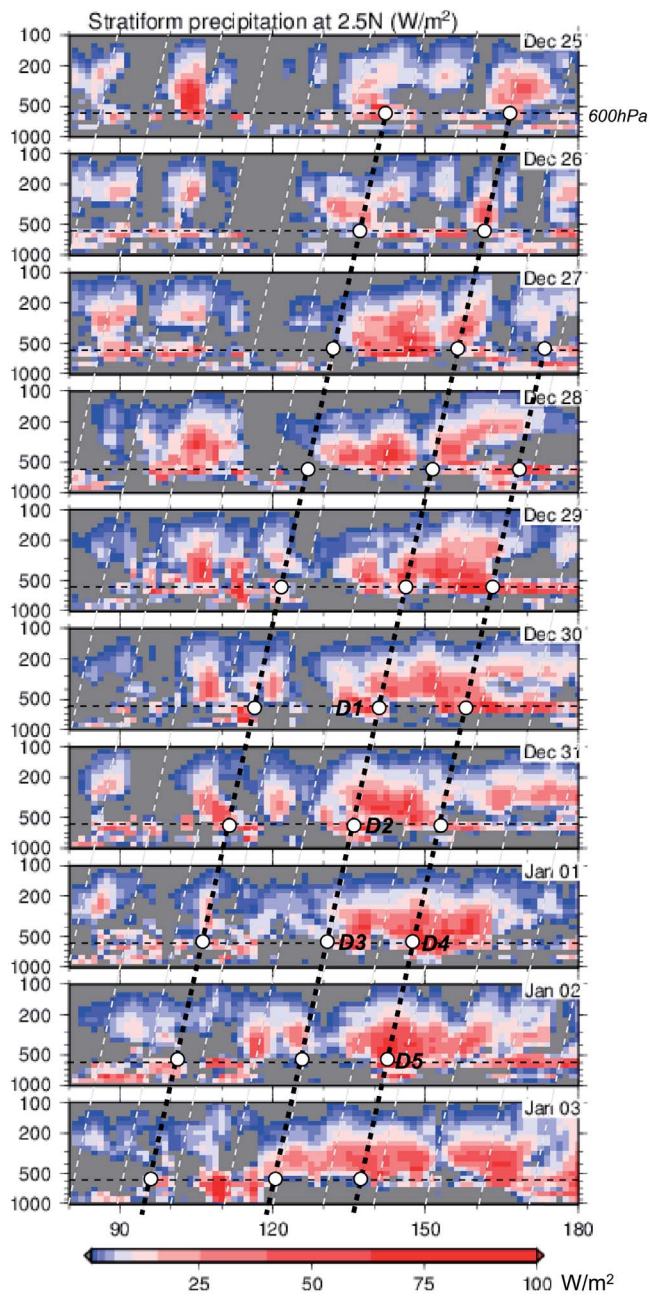


Figure 14. Vertical cross section of the simulated formation of stratiform precipitation sliced along 2.5°N . Broken lines with white circles and the labels D1–D5 are the same as in Figure 13.

the kinetic effect during evaporation from raindrops is likely to be small during active convection.

6. Summary and Discussion

[35] Clear intraseasonal isotopic variations associated with MJO convection were observed in satellite and ground-based station observations. Relatively high δD values were observed in water vapor during the pre-onset period and then became more depleted in mid-troposphere water during the MJO onset. A nudged-GCM with isotope tracers can

reasonably simulate the observed features of the isotopic evolution that accompanied the onset of an MJO event and was used to provide a mechanistic explanation of moist processes during MJO development.

[36] During the pre-onset period, surface evaporation is the dominant source of boundary-layer moisture. Because evaporative flux supplies moisture with relatively enriched isotopic ratios to the atmosphere, relatively higher isotope values are maintained in the boundary moisture. Convection carries this boundary moisture upward, where some of the moisture then detrains from the top of convective cloud. Because strong convective updraft transports condensed water upward before it precipitates, the isotopic value of detrained moisture is relatively enriched in heavy isotopes compared with the environmental values. Thus, because of convective detrainment, the isotopic content of the whole troposphere is characterized by relatively higher values than would be predicted by Rayleigh distillation.

[37] After the transition to deep convection, moisture with lower δD values than in the pre-onset period was noted in the middle and lower troposphere. During the MJO onset period, large-scale stratiform rainfall appeared, and the observed isotopic depletion was closely related with the convective–stratiform transition. The isotopic variation in surface water vapor was negatively correlated with increases in the stratiform area fraction, and thus the isotopic minima corresponded to maxima in stratiform rainfall (Figure 4). Satellite measurements confirmed that the lower δD values were displaced to the west of the center of deep convection during eastward propagation of the MJO cloud cluster (Figure 7a). The displacement matches with the westward-moving cloud shields that originate from the convective clouds (Figure 5c).

[38] The observed low δD values associated with stratiform precipitation were reasonably simulated by the nudged-GCM. In thick stratiform clouds, snowflakes and ice crystals with depleted isotopic content form in the upper troposphere and melt to become raindrops as they fall through and near clouds. Below the melting layer, diffusive exchange between raindrops and surrounding water vapor was found in the model to be the primary mechanism to explain the lower isotopic values of the water vapor. This interpretation is supported by the d-excess (d-value) tracer. While the d-values is relatively insensitive to liquid condensation occurring in thermal equilibrium, the d-excess profile in tropospheric moisture largely increases with altitude up to the upper troposphere because of ice formation at higher altitude. The δD minima found below the melting layer are accompanied by higher d-values. Under the cloud base, water vapor with low isotopic content and high d-values subside to lower levels and can influence the surface isotopic ratios during sustained stratiform precipitation. The simulated relationship between the isotopic depletion of surface water and the increase in d-value shows the origin of the vapor is from higher altitudes. This finding is consistent with the observed minimum δD value with the maximum d-value peak in the surface water during the maximum in stratiform rainfall (Figure 15).

[39] These results indicate that good simulation of the proportion of stratiform/convective rainfall is necessary for accurate simulation of water isotopes in the tropics. As shown by Lin *et al.* [2004], many GCMs significantly underestimate the proportion of stratiform rainfall. Fu and Wang [2009]

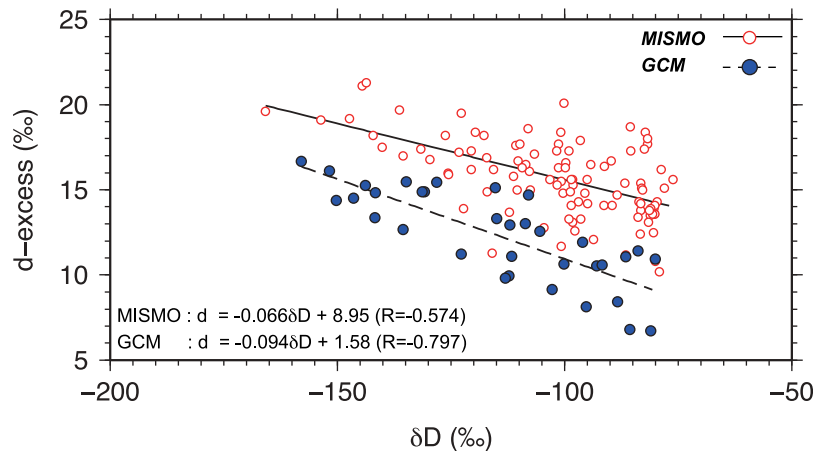


Figure 15. The δD - d -excess plots for water vapor in the boundary layer derived from R/V *Mirai* observations during the MISMO campaign (open red circle) and simulated by the nudged GCM, along with the MJO convection center shown as the gray line in Figure 7c (blue circle). Regression lines were calculated for each plot.

also emphasized that the representation of stratiform rainfall is necessary to robustly model the MJO. Thus, evaluation of the simulated proportion of stratiform/convective rainfall using isotope tracers is a potentially powerful tool to improve GCM simulations of the MJO. Additionally, isotopic tracers are sensitive to cloud microphysics. During the convective moistening period, the isotopic content of moisture detraining into the environment is sensitive to the precipitation efficiency, which controls the amount of condensation lifted in the convective plume. On the other hand, during the discharge period, isotopic depletion by diffusive exchange is sensitive to the amount of snow falling to the melting layer. Future isotopic profiles obtained by satellite may help improve our understanding of cloud microphysics and provide further insight into the MJO convection.

[40] Isotope tracers can be used not only at a large-scale, but also at smaller regional scales. The intensive ground-based observations described here showed short-term isotopic variations related to mesoscale structures of the MJO envelope. Although a high-resolution model that can reproduce mesoscale cloud structures will be required to evaluate the dominant moistening and dehydrating mechanisms, the application of isotopes provide a new hydrological perspective for understanding the vertical moisture transportation associated with the MJO, which aggregates into large-scale tropical convection systems.

Appendix A: Comparison of TES Retrieved δD to Model Output

[41] As described by Worden *et al.* [2006], to compare TES HDO/H₂O profiles with model output data, one must account for the instrument sensitivity, which depends on the atmospheric state (surface emissivity, temperature, humidity profiles, and clouds). Thus, we construct degraded model profiles using the TES instrument operator which convolves the GCM output with the TES averaging kernel constraint from the retrieval. In this study, to produce a model profile representing what TES would observed in a similar atmosphere, we applied the TES averaging kernel and a priori

constraint to daily model output following the method described by Worden *et al.* [2011]. The equations for the method have been explicitly described by Osterman *et al.* [2009] and in a form specific for the HDO/H₂O ratio by Risi *et al.* (submitted manuscript, 2011). As shown by Worden *et al.* [2011], the equivalent TES estimate of the HDO/H₂O profile for model output (\hat{x}_{model}) is written as follows:

$$\hat{x}_{model}^R = x_a^R + (A_{DD} - A_{HD})(x_{model}^D - x_a^D) - (A_{HH} - A_{DH})(x_{model}^H - x_a^H) \quad (A1)$$

where A_{DD} and A_{HH} are the averaging kernel matrices for HDO and H₂O, and A_{HD} and A_{DH} are the cross-term averaging kernels between HDO and H₂O and the reverse, respectively. The x^R , x^D , and x^H are the natural logarithm of the isotopic ratio (HDO/H₂O) and volume mixing ratios in HDO and H₂O, respectively. The x_{model} and x_a are the model and a priori constant vector profiles for each species. We re-gridded daily mean averaging kernels on the same grid as our model simulation (T106) and then applied output together with the a priori constant to our daily model.

[42] **Acknowledgments.** This research was supported by the Global Environment Research Fund RF-0083 of the Ministry of the Environment, Japan, and by grants from NASA Energy and Water cycle Study (07-NEWS07-0020) and the NASA Atmospheric Composition program (NNX08AR23G). We thank N. Sato for providing the OLR anomaly data, T. Ushiyama for providing the radar echo data, J. Worden for his help in designing the model-TES comparison methodology, D. Brown for his help in the TES data processing, and M. Berkelhammer for editing of this paper.

References

- Arakawa, A., and W. Shubert (1974), Interactions of cumulus cloud ensemble with the large-scale environment: Part I, *J. Atmos. Sci.*, *31*, 671–701.
- Benedict, J., and D. Randall (2007), Observed characteristics of the MJO relative to maximum rainfall, *J. Atmos. Sci.*, *64*, 2332–2354.
- Benedict, J., and D. Randall (2009), Structure of the Madden-Julian Oscillation in the superparameterized CAM, *J. Atmos. Sci.*, *66*, 3277–3296.
- Blade, I., and D. Hartmann (1994), Tropical intraseasonal oscillations in a simple nonlinear model, *J. Atmos. Sci.*, *51*, 2922–2939.
- Blossey, P., Z. Kuang, and D. Romps (2010), Isotopic composition of water in the tropical tropopause layer in cloud-resolving simulations of

- an idealized tropical circulation, *J. Geophys. Res.*, *115*, D24309, doi:10.1029/2010JD014554.
- Bony, S., C. Risi, and F. Vimeux (2008), Influence of convection processes on the isotopic composition ($\delta^{18}\text{O}$ and δD) of precipitation and water vapor in the tropics: 1. Radiative-convective equilibrium and Tropical Ocean-Global Atmosphere-Coupled Ocean-Atmosphere Response Experiment (TOGA-COARE) simulation, *J. Geophys. Res.*, *113*, D19305, doi:10.1029/2008JD009942.
- Chikira, M. (2010), A cumulus parameterization with state-dependent entrainment rate: Part II. Impact on climatology in a general circulation model, *J. Atmos. Sci.*, *67*, 2194–2211.
- Chikira, M., and M. Sugiyama (2010), A cumulus parameterization with state-dependent entrainment rate: Part I. Description and sensitivity to temperature and humidity profiles, *J. Atmos. Sci.*, *67*, 2171–2193.
- Craig, G., and L. Gordon (1965), Deuterium and oxygen 18 variation in the ocean and marine atmosphere, in *Stable Isotopes in Oceanographic Studies and Palaeotemperatures*, edited by E. Tongiorgi, pp. 9–130, Naz. delle Rich., Pisa, Italy.
- Dansgaard, W. (1964), Stable isotopes in precipitation, *Tellus*, *16*, 436–468.
- Field, R., D. Jones, and D. Brown (2010), The effects of post-condensation exchange on the isotopic composition of water in the atmosphere, *J. Geophys. Res.*, *115*, D24305, doi:10.1029/2010JD014334.
- Fu, X., and B. Wang (2009), Critical roles of the stratiform rainfall in sustaining the Madden-Julian Oscillation: GCM experiments, *J. Clim.*, *22*, 3939–3959.
- Hasumi, H., and S. Emori (Eds.) (2004), K-1 coupled GCM (MIROC) description, *Tech. Rep. 1*, Cent. for Clim. Syst. Res., Univ. of Tokyo, Tokyo.
- Hendon, H., and B. Liebmann (1994), Organization of convection within the Madden-Julian Oscillation, *J. Geophys. Res.*, *99*, 8073–8083.
- Hoffmann, G., M. Werner, and M. Heimann (1998), Water isotope module of the ECHAM atmospheric general circulation model: A study on timescales from days to several years, *J. Geophys. Res.*, *103*(D14), 16,871–16,896.
- Houze, J., R. A. (2004), Mesoscale convection systems, *Rev. Geophys.*, *42*, RG4003, doi:10.1029/2004RG000150.
- Hu, Q., and D. Randall (1994), Low-frequency oscillations in radiative-convective systems, *J. Atmos. Sci.*, *51*, 1089–1099.
- Jiang, X., et al. (2009), Vertical heating structures associated with the MJO as characterized by TRMM estimates, ECMWF reanalysis, and forecasts: A case study during 1998/99 winter, *J. Clim.*, *22*, 6001–6020.
- Johnson, D., K. Jucks, W. Traub, and K. Chance (2001), Isotopic composition of stratospheric water vapor: Measurements and photochemistry, *J. Geophys. Res.*, *106*(D11), 12,211–12,217.
- Jouzel, J. (1986), Isotopes in cloud physics: Multiphase and multistage condensation processes, in *Handbook of Environmental Isotope Geochemistry*, vol. 2, edited by P. Fritz and J. Fontes, chap. 2, pp. 61–112, Elsevier, New York.
- Jouzel, J., and L. Merlivat (1984), Deuterium and oxygen 18 in precipitation: Modeling of the isotopic effects during snow formation, *J. Geophys. Res.*, *89*, 11,749–11,757.
- Kemball-Cook, S., and B. Weare (2001), The onset of convection in the Madden-Julian Oscillation, *J. Clim.*, *14*, 780–793.
- Khairoutdinov, M., C. Demott, and D. Randall (2008), Evaluation of the simulated interannual and subseasonal variability in an AMIP-style simulation using the CSU multiscale modeling framework, *J. Clim.*, *21*, 413–431.
- Kiladis, G., K. Straub, and P. Haertel (2005), Zonal and vertical structure of the Madden-Julian Oscillation, *J. Atmos. Sci.*, *62*, 2790–2809.
- Kuang, Z., G. C. Toon, P. O. Wennberg, and Y. Yung (2003), Measured HDO/H₂O ratios across the tropical tropopause, *Geophys. Res. Lett.*, *30*(7), 1372, doi:10.1029/2003GL017023.
- Kurita, N., A. Sugimoto, Y. Fujii, T. Fukazawa, V. Makarov, O. Watanabe, K. Ichianagi, A. Numaguti, and N. Yoshida (2005), Isotopic composition and origin of snow over Siberia, *J. Geophys. Res.*, *110*, D13102, doi:10.1029/2004JD005053.
- Kurita, N., K. Ichianagi, J. Matsumoto, M. Yamanaka, and T. Ohata (2009), The relationship between the isotopic content of precipitation and the precipitation amount in tropical regions, *J. Geochem. Explor.*, *102*, 113–122.
- Lau, W., and D. Waliser (2005), *Intraseasonal Variability in the Atmosphere-Ocean Climate System*, 436 pp., Praxis, New York.
- Lawrence, J., and S. Gedzelman (1996), Low stable isotope ratios of tropical cyclone rains, *Geophys. Res. Lett.*, *23*, 527–530, doi:10.1029/96GL00425.
- Lawrence, J., S. Gedzelman, D. Dexheimer, H. Cho, G. Carrie, R. Gasparni, C. Anderson, K. Bowman, and M. Biggerstaff (2004), Stable isotopic composition of water vapor in the tropics, *J. Geophys. Res.*, *109*, D06115, doi:10.1029/2003JD004046.
- Lee, J., J. Worden, K. Bowman, A. Eldering, J.-L. F. LeGrande, A. Li, G. A. Schmidt, and H. Sodeman (2011), Relating tropical ocean clouds to moist processes using water vapor isotope measurement, *Atmos. Chem. Phys.*, *11*, 741–752, doi:10.5194/acp-11-741-752.
- Le Treut, H., and Z. Li (1991), Sensitivity of an atmospheric general circulation model to prescribed SST changes: Feedback effects associated with the simulation of cloud optical properties, *Clim. Dyn.*, *5*, 175–187.
- Lin, J., B. Mapes, M. Zhang, and M. Newman (2004), Stratiform precipitation, vertical heating profiles, and the Madden-Julian Oscillation, *J. Atmos. Sci.*, *61*, 296–309.
- Lin, J., et al. (2006), Tropical intraseasonal variability in 14 IPCC AR4 climate models: Part I. Convective signals, *J. Clim.*, *19*, 2665–2690.
- Madden, R., and P. Julian (1971), Detection of a 40–50 day oscillation in the zonal wind in the tropical Pacific, *J. Atmos. Sci.*, *28*, 702–708.
- Mapes, B. (2000), Convective inhibition, subgrid-scale triggering energy, and stratiform instability in a toy tropical wave model, *J. Atmos. Sci.*, *57*, 1515–1535.
- Mapes, B., and R. Houze (1993), Cloud clusters and superclusters over the oceanic warm pool, *Mon. Weather Rev.*, *121*, 1398–1415.
- Merlivat, L., and J. Jouzel (1979), Global climatic interpretation of the deuterium-oxygen 18 relationship for precipitation, *J. Geophys. Res.*, *84*, 5029–5033.
- Miura, H., M. Satoh, T. Nasuno, A. Noda, and K. Oouchi (2007), A Madden-Julian-Oscillation event realistically simulated by global cloud-resolving model, *Science*, *318*, 1763–1765.
- Nakazawa, T. (1988), Tropical super clusters within intraseasonal variations over the western Pacific, *J. Meteorol. Soc. Jpn.*, *66*, 823–839.
- Numaguti, A., M. Takahashi, T. Nakajima, and A. Sumi (1997), Description of CCSR/NIES atmospheric general circulation model, *CGER's Supercomputer Monogr. Rep.*, *3*, pp. 1–48, Cent. for Global Environ. Res., Natl. Inst. for Environ. Stud., Tsukuba, Japan.
- Onogi, K., et al. (2007), The JRA-25 reanalysis, *J. Meteorol. Soc. Jpn.*, *85*, 369–432.
- Osterman, G., et al. (2009), Level 2 Data User's Guide, version 4.0, *Tech. Rep. JPL D-38042*, Jet Propul. Lab., Calif. Inst. of Technol., Pasadena.
- Pan, D., and D. Randall (1998), A cumulus parameterization with a prognostic closure, *Quant. J. Meteorol. Soc.*, *124*, 949–981.
- Raymond, D. (2001), A new model of the Madden-Julian Oscillation, *J. Atmos. Sci.*, *58*, 2807–2819.
- Rayner, N., D. Parker, E. Horton, C. Folland, L. Alexander, D. Rowell, E. Kent, and A. Kaplan (2003), Global analyses of sea surface temperature, sea ice, and night marine air temperature since the late nineteenth century, *J. Geophys. Res.*, *108*(D14), 4407, doi:10.1029/2002JD002670.
- Schmidt, G. A., G. Hoffmann, D. Shindell, and Y. Hu (2005), Modeling atmospheric stable water isotopes and the potential for constraining cloud processes and stratosphere-troposphere water exchange, *J. Geophys. Res.*, *110*, D21314, doi:10.1029/2005JD005790.
- Slingo, J., et al. (1996), Intraseasonal oscillations in 15 atmospheric general circulation models: Results from an AMIP diagnostic subproject, *Clim. Dyn.*, *12*, 325–357.
- Smith, J., A. Ackerman, E. Jensen, and O. Toon (2006), Role of deep convection in establishing the isotopic composition of water vapor in the tropical transition layer, *Geophys. Res. Lett.*, *33*, L06812, doi:10.1029/2005GL024078.
- Stewart, M. (1975), Stable isotope fractionation due to evaporation and isotopic exchange of falling waterdrops: Applications to atmospheric processes and evaporation of lakes, *J. Geophys. Res.*, *80*(9), 1133–1146.
- Takemura, T., I. Uno, T. Nakajima, A. Higurashi, and I. Sano (2002), Modeling study of long-range transport of Asian dust and anthropogenic aerosols from East Asia, *Geophys. Res. Lett.*, *29*(24), 2158, doi:10.1029/2002GL016251.
- Thayer-Calder, K., and D. Randall (2009), The role of convective moistening in the Madden-Julian Oscillation, *J. Atmos. Sci.*, *66*, 3297–3312.
- Tian, B., D. Waliser, E. Fetzer, B. Lambrechtsen, Y. Yung, and B. Wang (2006), Vertical moist thermodynamic structure and spatial-temporal evolution of the MJO in AIRS observations, *J. Atmos. Sci.*, *63*, 2462–2485.
- Tokioka, T., K. Yamazaki, A. Kitoh, and T. Ose (1988), The equatorial 30–60-day oscillation and the Arakawa-Schubert penetrative cumulus parameterization, *J. Meteorol. Soc. Jpn.*, *66*, 883–901.
- Uno, I., K. Eguchi, K. Y. T. Takemura, A. Shimizu, M. Uematsu, Z. Liu, Z. Wang, Y. Hara, and N. Sugimoto (2009), Asian dust transported one full circuit around the globe, *Nat. Geosci.*, *2*, 557–560, doi:10.1038/NNGEO583.
- Waliser, D., et al. (2003), AGCM simulation of intraseasonal variability associated with the Asian summer monsoon, *Clim. Dyn.*, *21*, 423–446.
- Waliser, D., et al. (2009), MJO simulation diagnostics, *J. Clim.*, *22*, 3006–3030.

- Webster, C., and A. Heysfield (2003), Water isotope ratios D/H, $^{18}\text{O}/^{16}\text{O}$, $^{17}\text{O}/^{16}\text{O}$ in and out of clouds map dehydration pathways, *Science*, *302*, 1742–1746, doi:10.1126/science.1089496.
- Wheeler, M., and K. Weickmann (2001), Real-time monitoring and prediction of modes of coherent synoptic to intraseasonal tropical variability, *Mon. Weather Rev.*, *129*, 2677–2694.
- Worden, J., et al. (2006), Tropospheric emission spectrometer observations of the tropospheric HDO/H₂O ratio: Estimation approach and characterization, *J. Geophys. Res.*, *111*, D16309, doi:10.1029/2005JD006606.
- Worden, J., et al. (2007), Importance of rain evaporation and continental convection in the tropical water cycle, *Nature*, *445*, 528–532.
- Worden, J., D. Noone, J. Galewsky, A. Bailey, D. Brown, J. Hurley, S. Kulawik, J. Lee, and M. Strong (2011), Estimate of bias in Aura TES HDO/H₂O profiles from comparison of TES and in situ HDO/H₂O measurements at the Mauna Loa Observatory, *Atmos. Chem. Phys.*, *11*, 4491–4503, doi:10.5194/acp-11-4491-2011.
- Yamada, H., K. Yoneyama, M. Katsumata, and R. Shirooka (2010), Observation of a super cloud cluster accompanied by synoptic-scale eastward-propagating precipitating system over the Indian Ocean, *J. Atmos. Sci.*, *67*, 1456–1473.
- Yoneyama, K., et al. (2008), MISMO field experiment in the equatorial Indian Ocean, *Bull. Am. Meteorol. Soc.*, *89*, 1889–1903.
- Zhang, C. (2005), Madden-Julian Oscillation, *Rev. Geophys.*, *43*, RG2003, doi:10.1029/2004RG000158.
- Zhang, C., M. Dong, S. Gualdi, H. Hendon, E. Maloney, A. Marshall, K. Sperber, and W. Wang (2006), Simulations of the Madden-Julian oscillation in four pairs of coupled and uncoupled global models, *Clim. Dyn.*, *27*, 573–592.

N. Kurita, H. Yamada, and K. Yoneyama, Japan Agency for Marine-Earth Science and Technology (JAMSTEC), 2-15 Natsushima-cho, Yokosuka 237-0061, Japan. (nkurita@jamstec.go.jp)

D. Noone and C. Risi, Department of Atmospheric and Oceanic Science and Cooperative Institute for Research in Environmental Sciences, University of Colorado at Boulder, Boulder, CO 80309-0216, USA.

G. A. Schmidt, NASA Goddard Institute for Space Studies, 2880 Broadway, New York, NY 10025, USA.